

1 **Introduction**

2 Tropospheric ozone (O₃) is a secondary air pollutant, i.e. it is not emitted as such in the air but
3 it is formed by reactions among precursors (e.g. CH₄, VOCs, NO_x). Ozone is an important
4 greenhouse gas resulting in a direct radiative forcing of 0.35-0.37 W m⁻² on climate (Shindell
5 et al., 2009; Ainsworth et al., 2012). Despite significant control efforts and legislation to
6 reduce O₃ precursor emissions, tropospheric O₃ pollution is still a major air quality issue over
7 large regions of the globe (Lefohn et al., 2010; Langner et al., 2012; Young et al., 2013;
8 Cooper et al., 2014; EEA, 2015; Sicard et al., 2016a,b; Ochoa-Hueso et al., 2017). Long-range
9 transport of O₃ and its precursors can elevate the local and regional O₃ background
10 concentrations (Ellingsen et al., 2008; Wilson et al., 2012; Paoletti et al., 2014; Derwent et al.,
11 2015; Xing et al., 2015; Sicard et al., 2016a). Therefore, remote areas such as the Arctic
12 region can be affected (Langner et al., 2012). The current surface O₃ levels (35-50 ppb in the
13 northern hemisphere, NH) are high enough to damage both forests and crops by reducing
14 growth rates and productivity (Wittig et al., 2009; Anav et al., 2011; Mills et al., 2011;
15 Ashworth et al., 2013; Proietti et al., 2016).

16

17 Increasing atmospheric CO₂, nitrogen deposition and temperatures enhance plant growth, and
18 increase primary production and greening of plants (Nemani et al., 2003; Zhu et al., 2016). At
19 the global scale, a widespread increase of greening and net primary production (NPP) is
20 observed over 25-50% of the vegetated area, while a decrease is observed over only 7% of the
21 globe (Nemani et al., 2003; Zhu et al., 2016). In contrast, a previous modeling study over
22 Europe shows how surface O₃ reduces the mean annual gross primary production (GPP) by
23 about 22% and the leaf area index by 15-20% (Anav et al., 2011). Similarly, Proietti et al.
24 (2016), using different *in-situ* measurements collected over 37 European forest sites, found a
25 GPP decrease (up to 30%) caused by O₃ during the time period 2000-2010. At global scale,
26 over the time period 1901-2100, GPP is projected to decrease by 14-23% (Sitch et al., 2007).
27 As a consequence of reduced photosynthetic assimilation, the total biomass of trees is
28 estimated to be decreased by 7% under the current ground-level O₃ mean concentrations (40
29 ppb on average) and by 17% at mean O₃ concentrations expected in 2100 (97 ppb based on a
30 meta-analysis) compared to preindustrial O₃ levels in NH (about 10 ppb, Wittig et al., 2009).
31 From experiments, Wittig et al. (2009) also reported that the total tree biomass of
32 angiosperms was reduced by 23% at O₃ mean concentrations of 74 ppb, and by 7% at 92 ppb
33 for gymnosperms. High surface O₃ levels, exceeding 40 ppb, do occur in many regions of the
34 globe with associated economic costs of several billion dollars per year (Wang and Mauzerall,

35 2004; Ashmore, 2005). Ashworth et al. (2013) reported an annual loss of 3.5% for wheat
36 (very O₃-sensitive) and 1.0% for maize (more O₃-tolerant) for Europe in 2010 relative to
37 2000, while Holland et al. (2006) estimated a €4.5 billion loss in the production of 23
38 common crop species, due to surface O₃ exposure by 2020 relative to 2000.

39

40 The international Tropospheric Ozone Assessment Report (TOAR) establishes a state-of-the-
41 art of global O₃ metrics for climate change, human health and crop/ecosystem research
42 (Lefohn et al., 2017). To assess the potential O₃ risk and protect vegetation from O₃, different
43 metrics are used: the European and US standard (AOT40 and W126, respectively) are based
44 on exposure-based metrics, while flux-based metrics have been introduced only recently
45 (UNECE, 2010; Klingberg et al., 2014; EEA, 2015). Unlike the exposure-based metrics,
46 which only rely on the surface O₃ concentration, the flux-based metrics were developed to
47 quantify the accumulation of damaging O₃ taken up by vegetation through the stomata over a
48 species-specific phenological time-window. These metrics also provide an information-rich
49 tool in assessing the relative effectiveness of air pollution control strategies in lowering
50 surface O₃ levels worldwide (Monks et al., 2015). By reducing plant photosynthesis and
51 growth, high surface O₃ levels will result in reduction in carbon storage by vegetation, and
52 finally an indirect radiative forcing as a consequence of the CO₂ rising in the atmosphere
53 (Sitch et al., 2007; Ainsworth et al., 2012). This rising CO₂ reduces stomatal conductance
54 which decreases O₃ flux into plants leading to increased O₃ levels in the air of 3-4 ppb during
55 the growing season over the NH by doubling of CO₂ concentration (Fiscus et al., 2005;
56 Sanderson et al., 2007).

57

58 Projected changes in ground-level O₃ vary considerably among models (Stevenson et al.,
59 2006; Wild, 2007) and emission scenarios. In earlier studies, the emissions of O₃ precursors
60 were based on a high population growth, leading to very high projected surface O₃
61 concentrations by 2100 (Stevenson et al., 2000; Zeng and Pyle, 2003; Shindell et al., 2006).
62 The last emission scenarios, i.e. the Representative Concentration Pathways (RCPs) were
63 developed as part of the Fifth Assessment Report of the Intergovernmental Panel on Climate
64 Change (Meinshausen et al., 2011; van Vuuren et al., 2011; Cubasch et al., 2013; Myhre et
65 al., 2013). These scenarios include e.g. different assumptions on climate, energy access
66 policies, and land cover and land use changes (Arneth et al., 2008; Kawase et al., 2011;
67 Kirtman et al., 2013). Until now, studies on O₃ pollution impacts on terrestrial ecosystems are
68 either limited to a single model or to particular regions (e.g. Clifton et al., 2014; Rieder et al.,

69 2015) and only a few applications of global or regional models under the new RCPs scenarios
70 were carried out (Kelly et al., 2012). In the framework of the Atmospheric Chemistry and
71 Climate Model Intercomparison Project (ACCMIP), different simulations were performed by
72 Lamarque et al. (2013) and Young et al. (2013) from 16 global chemistry models.

73

74 A few issues about surface O₃, such as a better understanding of spatial changes and a better
75 assessment of O₃ impacts worldwide, are still challenging. To overcome these issues, the aim
76 of this study is to quantify, for the first time, the spatial and temporal changes in the projected
77 potential O₃ impacts on photosynthetic carbon assimilation of vegetation at global scale, by
78 comparing the O₃ potential injury at present with that expected at the end of the 21st century
79 from different global chemistry models. The purpose of this study is not to provide a
80 quantitative estimation of the ecosystem injury due to O₃ but to highlight the world areas at
81 higher risk and changes by 2100.

82

83 **Materials and Methods**

84

85 *ACCMIP models and RCP scenarios*

86

87 The global chemistry models used in this work were developed under the ACCMIP project. A
88 detailed description of the selected models and of the emission scenarios (i.e. RCPs) is
89 included in Supplementary Information (SI). ACCMIP models were widely validated and
90 used to evaluate projected changes in atmospheric chemistry and air quality under different
91 emission and climate assumptions (e.g. Lamarque et al., 2010; Fiore et al., 2012; Bowman et
92 al., 2013; Lee et al., 2013; Voulgarakis et al., 2013). Lamarque et al. (2013) and Young et al.
93 (2013) provided the main characteristics of 16 models and details for the ACCMIP
94 simulations. Although within the ACCMIP project 16 models are available, due to the lack of
95 hourly O₃ concentration here we only focus on 6 global chemistry models with different
96 configurations (Table 1).

97

98 The length of historical and RCP simulations vary between models, but for all models the
99 historical runs cover a period centered around 2000, while the time-slice of RCPs is centered
100 around 2100 (Table 1). As for each model we compare the relative mean change between the
101 historical and RCP simulations, a different length in the number of years used in the analysis
102 does not affect the results.

103

104 ***Potential ozone injury on vegetation***

105

106 The O₃ exposure-based index, i.e. AOT40 (ppb h), is a metric used to assess the potential O₃
107 risk to vegetation from local to global scales (Emberson et al., 2014). In literature, AOT40 is
108 computed as sum of the hourly exceedances above 40 ppb, for hours between 8:00 hours and
109 20:00 hours or for hours with a solar radiation exceeding 50 Wm⁻² over species-specific
110 growing seasons (UNECE, 2010). Conventionally, two major growing-season time windows
111 are used, i.e. six months (April to September) for temperate climates, e.g. in Europe and all-
112 year round for Mediterranean, subtropical and tropical-type climates where vegetation is
113 physiologically active all along the year (Paoletti et al., 2007).

114

115 UNECE (2010) supports the use of a growing season, but a fixed time-window does not allow
116 incorporating the changes in the growing season due to climate change and would thus not be
117 well suited when investigating changes over time. A recent study over Europe showed how
118 computing AOT40 only over the growing season (i.e. April-September) would lead to an
119 underestimation of AOT40 up to 50% for conifer trees, while in case of deciduous trees the
120 underestimation is much smaller (< 5%, Anav et al., 2016). Besides, it should be noted that in
121 Anav et al. (2016) the AOT40 is computed year-round. We computed the AOT40 for a model
122 grid for hours between 8:00 hours and 20:00 hours (local time) for all days of the year.
123 Therefore, we computed AOT40 as follows:

124

125
$$\text{AOT40} = \int_{01\text{jan}}^{31\text{dec}} \int_{8\text{am}}^{8\text{pm}} \max([\text{O}_3] - 40, 0) dt \quad (1)$$

126

127 where [O₃] is hourly O₃ concentration (ppb) simulated by the models at the lower model layer
128 and *dt* is time step (1h). The function "maximum" ensures that only values exceeding 40 ppb
129 are taken into account. For the protection of forests, a critical level of 5 ppm.h calculated over
130 the growing season is recommended by UNECE (2010). Within the 2008/50/CE Directive,
131 the critical level for agricultural crops (3ppm.h) is adopted as the long-term objective value
132 for the protection of vegetation by 2020.

133

134 The current chemistry models cannot predict changes in phenology over time, thus the
135 growing season length is the same between the historical period and different RCPs. The use
136 of a common fixed time-window (8-20h) all year-round at global level allows skipping the
137 use of a latitude model, which would increase the level of complexity and uncertainties.

138 Because the growing season is highly variable across the latitude, rather than introducing
139 further uncertainties by using a latitude model to simulate the growing season, we applied
140 here a simplified approach with a year-long growing season which should be considered as a
141 worst case study. This approach is valuable and can be easily applied at global scale to
142 compare the historical and projected potential risk to vegetation.

143
144 The O₃ concentration to be used in AOT40 calculation should be at the top of the canopy;
145 however, most of models used here provide O₃ concentrations at 90-120 m. Nevertheless,
146 even if the O₃ concentration is simulated at different elevations above the sea level, as for
147 each model we compare the variation between present and future, the change is consistent
148 because the elevation is the same. In case of risk assessment, by calculating AOT40 year-
149 round, an overestimation can be observed over polluted region of NH. Since the aim of this
150 study is to compare how O₃ stress to vegetation changes between historical period and future,
151 even if the AOT40 is misestimated at a given model grid point, as we compared the changes
152 in AOT40 at the same model grid point, the relative mean change is consistent.

153
154 From the AOT40, a factor of risk for forests and crops can be computed (Anav et al., 2011;
155 Proietti et al., 2016). Thus, the potential O₃ impact on photosynthetic carbon assimilation
156 (IO₃), in the worst-case scenario, is expressed through a dimensionless value as following:

$$157 \text{IO}_3 = \alpha \times \text{AOT40} \quad (2)$$

159
160 where α is an empirically derived O₃ response coefficient representing the proportional
161 change in net photosynthesis per unit of AOT40 (Anav et al., 2011). From the Global Land
162 Cover Facility (GLCF) data at 1° of spatial resolution, we grouped the vegetation in three
163 categories: conifers, crops (including grassland) and deciduous (including tropical forests and
164 shrubs) trees. Even, Dynamic Global Vegetation Models make use of plant functional types
165 rather than complex and specific vegetation to simulate shifts in potential vegetation as a
166 response to shifts in climate (Sitch et al., 2007). The relationships between cumulative ozone
167 exposure and reductions in net photosynthesis vary among and even within species (Reich,
168 1987; Ollinger et al., 1997). Differences in response per unit uptake tend to be greater in
169 magnitude between functional groups (e.g., hardwoods vs. conifers) where leaf structure and
170 plant growth strategy differ most widely (Reich, 1987). The dimensionless coefficient for
171 coniferous trees (0.7×10^{-6}) and crops (3.9×10^{-6}) are based on the regressions of the
172 photosynthesis response to O₃ (Reich, 1987), while the coefficient for deciduous trees

173 (2.6×10^{-6}) is based on Ollinger et al. (1997). From simulated changes in the risk factor, we
174 can highlight potential risk areas for vegetation.

175

176 **Results and Discussion**

177 Although differences in the simulated global O_3 spatial pattern were previously discussed and
178 analyzed (e.g. Lamarque et al., 2013), we show the mean annual O_3 concentration at the lower
179 model layer in Figure 1 because O_3 concentration explains AOT40 patterns. Then, in Figure 2
180 we show and discuss the AOT40 spatial and temporal distribution from the ACCMIP models
181 for the historical and RCPs simulations, and finally in Figure 3 we show the percentage of
182 variation of IO3, i.e. the change in the potential impact of O_3 on photosynthetic carbon
183 assimilation for the ACCMIP models computed comparing the RCPs simulations with
184 historical runs. All spatial averages were calculated over land surfaces. A detailed description
185 of each figure, model by model, is included in Supplementary Information (SI).

186

187 **Spatial pattern of historical ozone concentration and AOT40**

188 The highest surface O_3 concentrations (Fig. 1) and potential O_3 impacts (Fig. 2) are found in
189 the NH, highlighting a hemispheric asymmetry. The averaged values of global, NH and SH
190 mean surface O_3 , AOT40 and IO3 are derived from averaging values over the global/NH/SH
191 land areas only (Tables 3). AOT40 was used widely during the last two decades, not only in
192 Europe but also in South America (Moura et al., 2014) and Asia (Hoshika et al., 2011) when
193 environmental factors are not limiting, e.g. water availability, air temperature, solar radiation
194 affecting stomata opening (Anav et al., 2016; De Marco et al., 2016).

195

196 The multi-models O_3 mean concentration, averaged over the land points of the domain, is 37.9
197 ± 4.3 ppb in NH and 22.9 ± 3.8 ppb in SH (Table 3a). Over land surfaces, the NH extratropics
198 (i.e. mid-latitudes beyond the tropics) has 65% more O_3 than the SH extratropics (data not
199 shown). Similarly, the highest AOT40 values are found in the NH, with an averaged AOT40
200 of 24.8 ± 10.1 ppm.h in NH and 2.5 ± 1.7 ppm.h in SH (Table 3a).

201

202 According to previous studies, the annual mean background O_3 concentrations at NH mid-
203 latitudes range between 35 and 50 ppb during the end of the 20th century (e.g. Cooper et al.,
204 2012; IPCC, 2014; Lefohn et al., 2014). Similarly, we found historical surface O_3 mean
205 concentrations ranging between 35 and 50 ppb and 35-50 ppm.h for AOT40 in the NH, with

206 the highest values occurring over Greenland and in the latitude band 15-45°N, particularly
207 around the Mediterranean basin, Near East, Northern America and over the Tibetan plateau (>
208 50 ppb and 70 ppm.h) while the lowest O₃ burden (15-30 ppb, < 20 ppm.h) was recorded in
209 SH, particularly over Amazon, African and Indonesian rainforests where the O₃ dry
210 deposition rate is maximum, up to 1.80 cm s⁻¹ for mixed wood forests (Wesely and Hicks,
211 2000). Tropospheric O₃ has a significant source from stratospheric O₃ (Parrish et al., 2012)
212 and it can be transported by the large-scale Brewer-Dobson overturning circulation, i.e. an
213 upward motion from the tropics and downward at higher latitudes, resulting in higher O₃
214 concentrations in the extratropics (Hudson et al., 2006; Seidel et al., 2008; Parrish et al.,
215 2012). The six models are able to reproduce the spatial pattern of O₃ concentration and thus
216 AOT40 worldwide.

217

218 The highest historical O₃ mean concentrations are observed in GFDL-AM3 and the lowest are
219 found in MIROC-CHEM. In the early 2000s, the maximum global O₃ mean concentration (39
220 ppb) in GFDL-AM3 is associated to the lowest annual total NO_x emissions (46.2 Tg, Table
221 2a) and low LNO_x (4.4 Tg) while the minimum global O₃ mean concentration (28 ppb) in
222 MIROC-CHEM is related to the highest emissions of total NO_x per year (57.3 Tg) and
223 erroneously high LNO_x (9.7 Tg per year, Lamarque et al., 2013). MIROC-CHEM simulates
224 58 gaseous species in the chemical scheme with constant present-day biogenic VOCs
225 emissions while GFDL-AM3 simulates 81 species (Stevenson et al., 2012; Lamarque et al.,
226 2013). In GISS-E2-R, the hemispheric asymmetry in O₃ is more important with e.g. a mean
227 concentration of 22 ppb in SH and 42 ppb in NH. A stronger global AOT40 mean (26 ppm.h)
228 is observed in GISS-E2-R and the lowest (7 ppm.h) in MIROC-CHEM for historical
229 simulations. Model-to-model differences are observed due to different natural emissions of O₃
230 precursors (e.g. lightning NO_x) and the different chemical schemes used.

231

232 Higher O₃ burdens (mean concentration > 50 ppb, AOT40 >70 ppm.h) are simulated at high-
233 elevation areas, e.g. at Rocky and Appalachian Mountains and over the Tibetan plateau (Fig.
234 1, Fig. 2). At high-elevation, solar radiation, biogenic VOC emission, exchange between free
235 troposphere and boundary layer, and stratospheric O₃ intrusion within the troposphere are
236 more important than at the surface layer (Steinbacher et al., 2004; Kulkarni et al., 2011;
237 Lefohn et al., 2012). Altitude reduces the O₃ destruction by deposition and NO (Chevalier et
238 al., 2007). In addition, due to the high elevation, ambient air remains colder and dryer in
239 summer, leading to lower summertime O₃ losses from photolysis (Helmig et al., 2007). The

240 high-elevation areas, characterized by higher O₃ burdens, are well simulated in GISS-E2-R
241 and MOCAGE models.

242
243 The Tibetan plateau, so-called “ozone valley”, is the highest plateau in the world, with a mean
244 height of 4000 m a.s.l. (Tian et al., 2008) with strong thermal and dynamic influences on
245 regional and global climate (Chen et al., 2011). High surface O₃ mean concentrations (40-60
246 ppb) were reported in previous studies (e.g. Zhang et al., 2004; Bian et al., 2011; Guo et al.,
247 2015; Wang et al., 2015). Although this region is remote, road traffic, biofuel energy source,
248 coalmines and trash burning are prevalent. These pollution sources contribute to significant
249 amount of NO_x, CO and VOCs (Wang et al., 2015). The high O₃ levels are attributed to the
250 combined effects of high-elevation surface, thermal and dynamical forcing of the Tibetan
251 plateau and *in-situ* photochemical production in the air trapped in the plateau by surrounding
252 mountains (Guo et al., 2015; Wang et al., 2015). The dynamic effect, associated with the
253 large-scale circulation, is more important than the chemical effect (Tian et al., 2008; Liu et al.,
254 2010) and responsible for the high O₃ levels over the Tibetan plateau. The six models are able
255 to well reproduce the high surface O₃ mean concentrations (> 50 ppb) over the Tibetan
256 plateau.

257
258 Higher O₃ mean concentrations (> 60 ppb) are also observed in Southwestern U.S., at the
259 stations inland close to Los Angeles, in Northeastern U.S. and East Asia (e.g. Beijing) (Fig.
260 1). The American Southwest is an O₃ precursor hotspot where the industrial sources emit CH₄
261 and VOCs into the air (Jeričević et al., 2013) and the eastern and northern desert areas have
262 higher ambient O₃ than urban areas of southern California due to four factors: on-shore winds,
263 gasoline reformulation, eastward population expansion and nighttime air chemistry (Arbaugh
264 and Bytnerowicz, 2003). The surface concentrations show higher O₃ levels in areas downwind
265 of O₃ precursor sources, i.e. urban and well-industrialized areas, at distances of hundreds or
266 even thousands of kilometers due to transport of O₃ and precursors, including “reservoir”
267 species such as PAN, lower O₃ titration by NO and higher biogenic VOC emission (Wilson et
268 al., 2012; Paoletti et al., 2014; Monks et al., 2015; Sicard et al., 2016a). The higher O₃ levels
269 in areas downwind of O₃ precursor sources are well simulated in GISS-E2-R and MOCAGE
270 models.

271
272 Over Greenland, mean O₃ concentrations during the historical runs, ranged from 40 to 55 ppb
273 (Fig. 1) except in MIROC-CHEM (20-25 ppb). Similarly, Helmig et al. (2007) reported

274 annual mean of surface O₃ concentrations of 47 ppb over Greenland between 2000 and 2005,
275 particularly at the high-elevation Summit station (3200 m a.s.l.). Several investigations of
276 snow photochemical and oxidation processes over Greenland concluded that photochemical
277 O₃ production can be attributed to high levels of reactive compounds (e.g. oxidized nitrogen
278 species) present in the surface layer during the sunlit periods due to local sources e.g. NO_x
279 enhancement from snowpack emissions, peroxyacetyl nitrate (PAN) decomposition, boreal
280 forest fires or ship emissions (Granier et al., 2006; Stohl et al., 2007; Legrand et al., 2009;
281 Walker et al., 2012). PAN to NO_x ratio increases with increasing altitude and latitude (Singh
282 et al., 1992). The PAN reservoir for NO_x may be responsible for the increase in surface O₃
283 concentrations at high latitudes (Singh et al., 1992). Local O₃ production does not appear to
284 have an important contribution to the ambient high O₃ levels (Helmig et al., 2007), however
285 the long-range O₃ transport can elevate the background concentrations measured at remote
286 sites, e.g. Greenland (Ellingsen et al., 2008; Derwent et al., 2010). Low dry deposition rates
287 for O₃, from 0.01-0.05 cm s⁻¹ over oceans and snow, the downward transport of stratospheric
288 O₃, the photochemical local production and the large-scale transport (Zhang et al., 2003;
289 Legrand et al., 2009; Walker et al., 2012; Hess and Zbinden, 2013) are known factors to
290 explain higher O₃ pollution over Greenland.

291
292 The surface O₃ concentrations (> 40 ppb) and AOT40 (> 60 ppm.h) are higher over deserts,
293 downwind of O₃ precursor sources (e.g. Near East, Sierra Nevada, Colorado Desert), due to
294 lower O₃ dry deposition fluxes (Wesely and Hicks, 2000), O₃ precursors long-range transport
295 from urbanized areas and high insolation. Around the Mediterranean basin, elevated AOT40
296 values (> 60 ppm.h) are recorded, mainly due to the industrial development, road traffic
297 increment, high insolation, sea/land breeze recirculation and O₃ transport (Sicard et al., 2013).
298 All models, except MIROC-CHEM, are able to well reproduce the high surface O₃ mean
299 concentrations over Greenland and over deserts.

300 301 **Projected changes in ozone concentration and AOT40**

302
303 Recent studies display a mean global increase in background O₃ concentration from a current
304 level of 35-50 ppb (e.g. IPCC, 2014; Lefohn et al., 2014) to 55-65 ppb (e.g. Wittig et al.,
305 2007) and up to 85 ppb at NH mid-latitudes by 2100 (IPCC, 2014). During the latter half of
306 the 20th century surface O₃ concentrations have increased markedly at NH mid-latitudes (e.g.
307 Oltmans et al., 2006; Parrish et al., 2012; Paoletti et al., 2014), mainly related to increasing
308 anthropogenic precursor emissions related to economic growth of industrialized countries

309 (e.g. Lamarque et al., 2005). Our results indicate that the future projections of the mean
310 surface O₃ concentrations and AOT40 vary considerably with the different scenarios and
311 models (Fig. 1 and 2). The six models simulate a decrease of O₃ concentration by 2100 under
312 the RCP2.6 and RCP4.5 scenarios, and an increase under the RCP8.5 scenario (Lamarque et
313 al., 2011). In our study, the averaged relative changes in surface O₃ concentration means (and
314 AOT40) for the different RCPs are: -21% (-75%) for RCP2.6, - 10% (-50%) for RCP4.5 and
315 + 14% (+69%) for RCP8.5 with a strong disparity between both hemispheres, e.g. - 8% in SH
316 and - 25% in NH for RCP2.6 (Tables 3b-c). RCP8.5 is the only scenario to show an increase
317 in global background O₃ levels by 2100 (+ 23% in SH and + 11% in NH).

318
319 Under the RCP2.6 scenario, all models predict that surface O₃ will strongly decrease
320 worldwide, except in Equatorial Africa where higher O₃ levels are observed in GFDL-AM3,
321 GISS-E2-R and MOCAGE. In CESM-CAM, GFDL-AM3 and MIROC-CHEM, a
322 homogeneous decrease in O₃ burden is simulated worldwide while in GISS-E2-R, MOCAGE
323 and UM-CAM, the strongest decrease in surface O₃ mean concentrations are found where
324 high historical O₃ concentrations were reported. Under RCP4.5 scenario, the surface O₃ mean
325 concentrations and AOT40 values are lower than historical runs worldwide for all models
326 except in MOCAGE where deterioration is observed over Canada, Greenland and East Asia.
327 For all models, the surface O₃ levels and AOT40 are higher for RCP8.5 as compared to
328 historical runs and the highest increases occur in the North-western America, Greenland,
329 Mediterranean basin, Near East and East Asia. The AOT40 values, exceeding 70 ppm.h, are
330 found over the Tibetan plateau and in Near East and over Greenland. For RCP8.5, GFDL-
331 AM3 is the most pessimistic model and MIROC-CHEM the most optimistic. By the end of
332 the 21st century, similar patterns are evident for RCP4.5 compared to RCP2.6 and RCP4.5
333 simulation is intermediate between RCP2.6 and RCP8.5 ones.

334
335 For all models and RCPs, the O₃ hot-spots (mean concentrations > 50 ppb and AOT40 > 70
336 ppm.h) are over Greenland and South Asia, in particular over the Tibetan plateau. The highest
337 increases are observed in NH, in particular in North-western America, Greenland, Near East
338 and South Asia (> 65 ppb). For the three RCPs, no significant change in ground-level O₃ is
339 observed in SH and the SH extratropics makes a small contribution to the overall change.

340
341 A recent global study showed the geographical patterns of surface air temperature differences
342 for late 21st century relative to the historical run (1986-2005) in all RCP scenarios (Nazarenko

343 et al., 2015). The global warming in the RCP2.6 scenario is 2-3 times smaller than RCP4.5
344 scenario and 4-5 times smaller than RCP8.5 scenario (Nazarenko et al., 2015). For the three
345 RCPs, the greatest change is observed over the Arctic, above latitude 60°N, and in the latitude
346 band 15-45°N (IPCC, 2014; Nazarenko et al., 2015). The least warming is simulated over the
347 large area of the Southern Ocean. For RCP8.5 scenario, the global pattern of surface O₃ levels
348 and AOT40 (Fig. 1-2) is similar to surface air temperature increase distribution. For RCP8.5,
349 significant increases in air temperature are simulated over latitude 60°N and over the Tibetan
350 plateau (more than 5°C). An increase of 4-5°C over the Near East, East and South Asia, North
351 and South Africa and Canada are simulated as well as + 1-3°C for the rest of the world
352 (Nazarenko et al., 2015). The tropospheric warming is stronger in the latitude band 15-45°N
353 (Seidel et al., 2008) and Hudson et al. (2006) have demonstrated that O₃ trends over a 24-year
354 period in the NH are due to trends in the relative area of the tropics and mid-latitudes and
355 Polar Regions. All models are able to reproduce the global pattern of air temperature changes
356 distribution in agreement with surface O₃ concentrations changes.

357

358 The spread in precursor emissions (e.g. VOCs, NO_x, CO) is due to the range of representation
359 of biogenic emissions (NO_x from soils and lightning, CO from oceans and vegetation) as well
360 as the complexity of chemical schemes in particular for NMVOCs simulations (e.g. isoprene)
361 from explicitly specified to fully interactive with climate. RCP2.6 scenario has the lowest O₃
362 precursor concentrations, and RCP8.5 has relatively low NO_x, CO and VOCs emissions, but
363 very high CH₄ (Table 2b). The global emissions of NO_x (-44%), VOCs (-5%) CO (-40%) and
364 CH₄ burden (-27%) decline, while LNO_x increase by e.g. 7% under RCP2.6 (Table 2b). The
365 CO (-32%) and NO_x (-20%) emissions have decreased while LNO_x (+33%), VOCS (+1%)
366 and CH₄ burden have increased (+120%) under RCP8.5 scenario (Table 2b). The GISS-E2-R
367 model shows a greater degree of variation than other models, with a stronger increase in CH₄
368 burden (+ 153%) and in VOCs emissions (+ 20%) for RCP8.5 (Table 2b).

369

370 Excluding CH₄ burden and VOCs emissions, all the RCP scenarios include reductions and
371 redistributions of O₃ precursor emissions throughout the 21st century, due to the air pollution
372 control strategies worldwide. The changes in CH₄ burden are due to the different climate
373 policies in model assumptions. In RCP2.6, CH₄ emissions decrease steadily throughout the
374 century, in RCP4.5 it remain steady until 2050 and then decrease (Voulgarakis et al., 2013)
375 and in RCP8.5 (no climate policy) it rapidly increase compared to 2000. Methane burdens are
376 fixed in the models with no sources, except for the GISS-E2-R simulations in which surface

377 CH₄ emissions are prescribed for future rather than concentrations (Shindell et al., 2012). The
378 model chemical schemes vary greatly in their complexity, mainly due to the NMVOCs
379 simulations (Young et al., 2013). Isoprene dominates the total NMVOCs emissions (Guenther
380 et al., 1995). In contrast to other models with constant present-day isoprene emissions, the
381 GISS-ES2-R simulations incorporate climate-driven isoprene emissions, with greater BVOC
382 emissions by 2100 and a positive change in total VOCs emissions across RCPs, related to the
383 positive correlation between air temperature and isoprene emission (e.g. Guenther et al., 2006;
384 Arneth et al., 2011; Young et al., 2013).

385
386 For RCP2.6 and RCP4.5 scenarios, there is a widespread decrease in O₃ in NH by 2100. The
387 overall decrease in O₃ concentration and AOT40 means for RCP4.5 are about half of that
388 between RCP2.6 and the historical simulation. For both scenarios, the changes are dominated
389 by the decrease in O₃ precursor emissions in the NH extratropics compared to historical
390 simulations (Table 2b). In NO_x saturated areas, annual mean O₃ will slightly increase as a
391 result of a less efficient titration by NO, but the overall O₃ burden will decrease substantially
392 at hemispheric scale over time (Gao et al., 2013; Querol et al., 2014; Sicard et al., 2016a). In
393 RCP4.5, Gao et al. (2013) showed that the largest decrease in O₃ (4-10 ppb) occurs in summer
394 at mid-latitudes in the lower troposphere while the O₃ concentrations undergo an increase in
395 winter. During the warm period, the photochemistry plays a major role in the O₃ production,
396 suggesting that the reduction in surface O₃ concentrations is in agreement with the large
397 reduction in anthropogenic O₃ precursor emissions (Sicard et al., 2016a) reducing the extent
398 of regional photochemical O₃ formation (e.g. Derwent et al., 2013; Simpson et al., 2014).
399 Titration effect was also reported by Collette et al. (2012) over Europe by using six chemistry
400 transport models.

401
402 The O₃ increase can be also driven by the net impacts of climate change, i.e. increase in
403 stratospheric O₃ intrusion, changing LNO_x and impacting reaction rates, through sea surface
404 temperatures and relative humidity changes (Lau et al., 2006; Voulgarakis et al., 2013; Young
405 et al., 2013).

406
407 Under the RCP8.5 scenario, the increase in surface O₃ concentrations, by 14% on average, can
408 be attributed to the higher CH₄ emissions coupled with a strong global warming, exceeding
409 2°C, and a weakened NO titration by reducing NO_x emissions (Stevenson et al., 2013; Young
410 et al., 2013). The global CH₄ burden are 27% and 5% lower than 2000, for the RCP2.6 and

411 RCP4.5 scenarios respectively while for RCP8.5, the total CH₄ burden has more than doubled
412 compared to early 2000s and LNO_x emissions increased by 33% (Table 2b). In addition,
413 stronger increases are found over the high-elevation Himalayan Plateau reflecting increased
414 exchange with the free troposphere or stratosphere (Lefohn et al., 2012; Schnell et al., 2016).
415 Several studies reported an increase in the stratospheric O₃ influx and higher stratospheric O₃
416 levels in response to a warming climate (e.g. Hegglin and Shepherd, 2009; Zeng et al., 2010).
417 The downwards O₃ transport from the stratosphere is an important source of tropospheric O₃
418 (Hsu and Prather, 2009; Tang et al., 2011), therefore, stratospheric O₃ recovery also plays a
419 partial role (e.g. + 11% for RCP8.5) in surface O₃ burden pattern. As an example, in
420 MOCAGE, smaller reduction in global O₃ mean concentrations (-13%) and higher increase in
421 stratospheric O₃ inputs (+20%) are observed for RCP2.6 (Table 3b). Similarly, for RCP8.5,
422 the highest increase in O₃ mean concentrations (+23%) and stratospheric O₃ (+24%) are
423 recorded in MOCAGE. In addition, lightning NO_x emissions show significant upward trend
424 from 2000 to 2100, in particular for the strongest warming scenario (RCP8.5) with greater
425 convective and lightning activity (e.g. Williams, 2009; Lamarque et al., 2013). For RCP8.5, a
426 reduction in surface O₃ concentrations is also simulated over the equatorial region, where the
427 increased relative humidity, in a warmer climate, increases the O₃ loss rate (e.g. Johnson et
428 al., 1999; Zeng and Pyle, 2003).

429

430 For RCP2.6 and RCP4.5, absolute decreases are observed for the Mediterranean basin and the
431 Western U.S. due to less precursor emissions in the NH extratropics (e.g. reduction of 5-7 ppb
432 over Europe). Smaller reduction in surface O₃ levels in South and East Asia highlight the
433 smaller changes in O₃ precursor emissions due to the recent emission growth in this region
434 (e.g. Zhang et al., 2009; Xing et al., 2015). For RCP 8.5, the high O₃ increase (up to 10 ppb)
435 in South Asia can be attributed to substantial increase in CH₄ emissions coupled with a strong
436 global warming, exceeding 2°C, and a weakened NO titration and a greater stratospheric O₃
437 influx (Kawase et al., 2011; Wild et al., 2012; Young et al., 2013).

438

439 **Risk areas for vegetation under RCP scenarios**

440

441 Figure 3 shows the changes in the potential O₃ impact on photosynthetic carbon assimilation
442 between present and future. It should be noted that a zero percentage of change (i.e. no
443 change) for IO₃, is simulated in sparsely vegetated regions (e.g. Gobi, Sahara, Near East,
444 Western plateau and Greenland), while the change can be higher than 100% when the
445 historical O₃ concentrations are lower than 40 ppb (i.e. AOT₄₀ = 0 and IO₃ = 0) and the O₃

446 concentrations exceed 40 ppb under RCPs (i.e. $AOT_{40} > 0$, $IO_3 > 0$). If the AOT_{40} during
447 the historical period is 0 then the percentage of change is undefined and we have considered
448 and set these grid points as missing values.

449

450 The potential O_3 impact for vegetation strongly decreases in NH for RCP2.6, except in
451 MOCAGE where a slight increase in the risk factor (+ 15 %) is simulated at high latitudes and
452 in South Asia. Conversely, the areas where the risk for vegetation increases (> 60 %) occur
453 over Africa (+ 15% to + 60%) for all models, except in CESM-CAM where no change is
454 observed across Africa. Under RCP4.5 scenario, the strongest increase in potential risk for
455 vegetation ($> + 60$ %) is simulated by MOCAGE, markedly different from the other models,
456 above the latitude $50^\circ N$. For all models, the potential O_3 impact for vegetation increases
457 across Africa, from - 15% to + 60% while slight decreases or no change occur worldwide.
458 Under RCP8.5 scenario, an increase of average O_3 over a significant part of the domain is
459 simulated, therefore the exposure to O_3 pollution and impacts on vegetation will increase
460 worldwide by 2100. An increase of the O_3 impacts on vegetation is simulated in Northern
461 U.S., South America, Asia and Africa while a reduction in particular over Eastern U.S. and
462 Southeastern China, and a slight increase (+ 15%) or decrease (- 15%) over Europe depending
463 on the model, are simulated.

464 In summary, compared to the historical simulations, the averaged relative changes in the O_3
465 risk factor for the different RCPs are: - 61% for RCP2.6, - 47% for RCP4.5 and + 70% for
466 RCP8.5 (Table 3d). We thus find a significant reduction in risk for vegetation for both
467 RCP2.6 and RCP4.5 scenarios, except in South Africa and at high-latitudes in MOCAGE
468 simulations, and a strong increase in global risk under RCP8.5. Under RCP2.6 and RCP4.5
469 scenarios, IO_3 slightly increases in Africa and over North America and Asia ($>$ latitude $60^\circ N$)
470 in MOCAGE. The risk increases over the few areas where the O_3 concentrations increased
471 between the historical period and 2100. Under both scenarios, the strongest reductions in risk
472 are observed over Amazon, Central Africa and South Asia, i.e. where the O_3 concentrations
473 have strongly declined between historical period and 2100. Under the RCP8.5, the areas
474 where the highest projected O_3 mean concentrations are simulated (e.g. Greenland, deserts)
475 are not associated with an increase in IO_3 due to the absence of vegetation. Under RCP8.5,
476 IO_3 increases worldwide while a reduction is simulated over Southeast North America,
477 northern Amazon, Central Africa and Southeast Asia, and a slighter reduction or a slight
478 increase is simulated over Western Europe (depending on the model).

479

480 The spatial pattern of IO₃ is consistent with previous analyses on global environmental
481 changes (climate, land-cover, nitrogen deposition, CO₂ fertilization) impacts on vegetation
482 (Nemani et al., 2003; Zhu et al., 2016), i.e. the highest reduction in risk for vegetation, in
483 particular under RCP8.5, occurs over areas where a strong increase in greening, LAI and NPP
484 is observed due to global changes and where a reduction in surface O₃ mean concentrations is
485 found by 2100 (Fig. 1). The regions with the largest greening trends are in Southeast North
486 America, northern Amazon, Europe, Central Africa and Southeast Asia with an average
487 increase of the observed LAI exceeding 0.25 m² m⁻² per year (Zhu et al., 2016). The CO₂
488 fertilization effects (70%), nitrogen deposition (9%) and climate change (8%) explain the
489 observed greening trend (Zhu et al., 2016). The changing climate alone produces persistent
490 NPP increases and the regions with the highest increase in NPP, ranging from 1.0-1.5% per
491 year, are in Southeast North America, northern Amazon, Western Europe, Central Africa and
492 South Asia (Nemani et al., 2003). From 1982 to 1999, the highest increases are observed in
493 tropical regions, with more than 1.5% per year over Amazon rainforest which accounts for
494 42% of the global NPP increase (Nemani et al., 2003). Amazon rainforest is one region where
495 the effects are statistically significant. This is particularly important owing to the role of the
496 Amazon rainforests in the global carbon cycle (Zhu et al., 2016). In these areas, we observed a
497 strong increase in NPP and LAI due to warming climate while a reduction in GPP (from - 10
498 to - 20%) due to O₃ is observed (Sitch et al., 2007). Inversely, the risk for vegetation IO₃
499 increases in particular in Africa, e.g. western Africa along the Gulf of Guinea, in South Brazil
500 and over high-latitudes regions (> 60°N) in North America and Asia where a reduction or a
501 slight increase in LAI (from - 0.05 to + 0.03 m² m⁻² per year) and strong decreases in NPP
502 (1.0-1.5% per year) are simulated (Nemani et al., 2003; Zhu et al., 2016).

503

504 Sitch et al. (2007) reported a high GPP reduction due to O₃ effects, between 1901 and 2100
505 under the *Special Report on Emissions Scenarios A2 emissions* scenario, exceeding 30% in
506 summer over Western Europe, Eastern North America, Amazon, central Africa and South
507 Asia. Previous studies reported that the reductions in GPP simulated by Sitch et al. (2007) are
508 overestimated up to six times due to i) the lack of empirical data about the response of
509 different species to O₃, Sitch et al. (2007) focused on broad-leaved tree, needle-leaved tree, C3
510 crops, C4 crops and shrubs; ii) the fact that a few experiments have shown no response, e.g.
511 grasslands (Bassin et al., 2013) and iii) the non-inclusion of the nitrogen limitation of growth
512 (Ren et al., 2011; Zak et al., 2011; Kvaleveg and Myhre 2013). In addition, the simulated O₃

513 concentrations over Amazon forest exceed 90 ppb in summer in Sitch et al. (2007) while the
514 annual O₃ mean is around 15-20 ppb by 2100 in our study.

515
516 The projected land covers widely vary under RCPs (Betts et al., 2015). In RCP2.6 scenario,
517 the ground surface covered by croplands increases as a result of bio-energy production, with a
518 more-or-less constant use of grassland. The RCP4.5 scenario focuses on global reforestation
519 programs as part of global climate policy, as a result, the use of cropland and grassland
520 decreases. Under RCP8.5, an increase in croplands and grasslands is applied mostly driven by
521 an increasing global population (van Vuuren et al., 2011). About 50% of forests, grasslands
522 and croplands might be exposed to high O₃ levels by the end of the 21st century (Sitch et al.,
523 2007; Wittig et al., 2009).

524 Generally, deciduous broadleaf are highly O₃-sensitive risk areas and needleleaf forests are
525 moderately O₃-sensitive risk areas. Crops and grasslands are more sensitive to O₃ exposure
526 than trees and deciduous trees are more sensitive than coniferous trees with lower stomatal
527 conductance (Felzer et al., 2004; Ren et al., 2007; Wittig et al., 2009; Anav et al., 2011).
528 Based on a comparison between Figure 2 and the Global Land Cover Facility maps, we can
529 observe that generally the AOT40, i.e. the potential O₃ risk to vegetation is high over
530 shrublands (e.g. high-latitude region), broadleaf forests (e.g. central Africa), needleleaf forests
531 (e.g. North America) and crops (e.g. South Asia). Under RCP2.6 and RCP4.5, the risk
532 decreases over areas covered by shrublands, savannas and slightly decreases over areas with
533 needleleaf forests in Northern America and Northern Asia. The risk strongly increases over
534 broadleaf forest in Africa and the risk slightly decreases or slightly increases over grasslands
535 (Central Asia and central Africa and U.S.). Under RCP8.5, the largest decreases in risks occur
536 in Eastern U.S., Europe and South-eastern China, where the ground is mainly dominated by
537 croplands, in all models except CESM-CAM.

538 **Conclusions**

539 From six global atmospheric chemistry transport models, we illustrate the changes, i.e.
540 differences for late 21st century relative to the historical run, in ground-level O₃
541 concentrations and vegetation impact metric (AOT40). Finally, the potential O₃ impacts on
542 photosynthetic carbon assimilation worldwide are investigated to define potential risk areas
543 for vegetation at global scale by 2100. A major advantage of this study is a comparison
544 between models and scenarios to explore future potential O₃ impacts.

545

546 The six models are able to well reproduce the spatial pattern of historical O₃ concentration
547 and AOT40 at global scale, in particular GISS-E2-R and MOCAGE are able to simulate the
548 higher O₃ levels in areas downwind of precursor sources and at the high-elevation areas. The
549 model outputs emphasize the strong asymmetry in the tropospheric O₃ distribution between
550 NH and SH. The natural emissions of O₃ precursors (e.g. lightning NO_x, CO from oceans,
551 isoprene) as well as the complexity of chemical schemes are significant sources of model-to-
552 model differences.

553

554 Compared to early 2000s, the results suggest changes in surface O₃ of -9.5 ± 2.0 ppb (NH)
555 and -1.8 ± 2.1 ppb (SH) in the cleaner RCP2.6 scenario and of $+4.4 \pm 2.8$ ppb (NH) and $+5.1 \pm 2.1$ ppb (SH) in RCP8.5 scenario. For RCP2.6 and RCP4.5, absolute decreases are
556 observed for the Mediterranean basin and the Western U.S. due to less precursor emissions in
557 the NH extratropics. For RCP8.5, all models show climate-driven increases in ground-level
558 O₃ in particular over the Western U.S, Greenland, South Asia and Northeast China and the
559 changes ranged from $+1-5$ ppb over North America and Europe. This O₃ increase can be
560 mainly attributed to substantial increase in CH₄ emissions coupled with a global warming and
561 a weakened NO titration
562

563

564 Most important results from the study are the spatial patterns and projected changes in global
565 AOT40 and risk areas for vegetation under the RCP scenarios. Even if AOT40 was computed
566 year-round, the global models suggest that despite an improvement under RCP2.6 and
567 RCP4.5, the AOT40-based critical levels for the protection of forests and crops will be
568 exceeded over many areas of the NH and they may be much more exceeded under RCP8.5 up
569 to a factor exceeding 10 by 2100.

570

571

572 Ozone may be a major threat to biodiversity over large regions of the world, however the size
573 of these areas remains uncertain. The potential O₃ impact on carbon assimilation, IO₃,
574 provides a clear indicator of the potential risk to vegetation. By 2100, the potential O₃ impact
575 on photosynthetic carbon assimilation decreases by 61% and 47% under RCP2.6 and RCP4.5,
576 respectively and increases by 70% under RCP8.5, compared to early 2000s over the whole
577 domain.. The strongest increase of the O₃ impacts on vegetation is simulated in Northern

578 America and Asia and central Africa. The highest reduction in risk for vegetation (i.e.
579 Southeast North America, the northern Amazon, Central Africa and Southeast Asia) occurs
580 over areas where a strong increase in greening, LAI and NPP is observed and where a
581 reduction in O₃ mean concentrations is found by 2100.

582 Many ecosystems worldwide are unprotected from O₃ due to the lack of international efforts
583 (Emberson et al., 2014). An efficient reduction in overall O₃ levels is expected over North
584 America and Europe in all RCP scenarios and worldwide if CH₄ emissions are reduced (e.g.
585 Kirtman et al., 2013; Pfister et al., 2014; Schnell et al., 2016). To efficiently protect vegetation
586 against O₃ pollution, suitable standards are urgently needed and the mitigation actions must be
587 as part of international emission reduction programmes. The flux-based metric is introduced
588 as new standard for vegetation protection against effects of O₃, taking into account the
589 detoxification processes and the modifying effects of multiple climatic and phenological
590 factors on O₃ uptake (Paoletti and Manning, 2007; Sicard et al., 2016b,c). Plant phenology
591 plays a pivotal role in the climate system as it regulates the gas exchange between the
592 biosphere and the atmosphere. Currently, in many O₃ risk assessment studies, the phenology
593 function is based on a simple latitude and topography model and the chemistry models do not
594 take into account the shifts in plant phenology and in start and end date of the growing season;
595 however a first attempt to study the role of phenology on stomatal ozone uptake is shown by
596 Anav et al (2017).

597

598 **Acknowledgements**

599 This work was carried out with the contribution of the LIFE financial instrument of the
600 European Union (LIFE15 ENV/IT/183) in the framework of the MOTTLES project
601 “Monitoring ozone injury for setting new critical levels” and published within the
602 International Union of Forest Research Organizations (IUFRO) Task Force on Climate
603 Change and Forest Health and IUFRO RG 7.01.09 “Ground-level ozone”.

604

605 **Bibliographic references**

- 606 **Ainsworth E.A.**, Yendrek C.R., Sitch S., Collins, W.J., Emberson L.D., 2012, “The effect of
607 Tropospheric Ozone on Net Primary Productivity and Implications for Climate Change”.
608 *Annu. Rev. Plant Biol.* 63: 637-661
- 609 **Anav A.**, Liu Q., De Marco A., Proietti C., Savi F., Paoletti E., Piao S., 2017, “The role of
610 plant phenology in stomatal ozone flux modelling”. *Global Change Biol.* doi:
611 10.1111/gcb.13823
- 612 **Anav A.**, Menut L., Khvorostyanov D., Viovy N., 2011, “Impact of tropospheric ozone on the
613 Euro-Mediterranean vegetation”. *Global Change Biol.* 17: 2342-2359
- 614 **Arbaugh M.J.**, and Bytnerowicz A., 2003, “Ambient ozone patterns and effects over the
615 Sierra Nevada: synthesis and implications for future research”. In: A. Bytnerowicz, M.
616 Arbaugh, R. Alonso (eds), *Ozone Air Pollution in the Sierra Nevada: Distribution and Effects*
617 *on Forests, Developments in Environmental Science*, vol. 2, Elsevier, Amsterdam, 249-261
- 618 **Arnth A.**, Schurgers G., Lathièrè J., Duhl T., Beerling D. J., et al., 2011, “Global terrestrial
619 isoprene emission models: sensitivity to variability in climate and vegetation”. *Atmos. Chem.*
620 *Phys.* 11: 8037-8052
- 621 **Arnth A.**, Schurgers G., Hickler T., Miller P.A., 2008, “Effects of species composition, land
622 surface cover, CO₂ concentration and climate on isoprene emissions from European forests”.
623 *Plant Biol.* 10: 150-162
- 624 **Ashmore M.R.**, 2005, “Assessing the future global impacts of ozone on vegetation”. *Plant*
625 *Cell Environ.* 28: 949-964
- 626 **Ashworth K.**, Wild O., Hewitt C.N., 2013, “Impacts of biofuel cultivation on mortality and
627 crop yields”. *Nat. Clim. Change* 3: 492-496
- 628 **Bassin S.**, Volk M., Fuhrer J., 2013, “Species composition of subalpine grassland is sensitive
629 to nitrogen deposition, but not ozone, after seven years of treatment”. *Ecosystems* 16: 1105-
630 1117
- 631 **Betts R.A.**, Golding N., Gonzalez P., Gornall J., Kahana R., et al., 2015, “Climate and land
632 use change impacts on global terrestrial ecosystems and river flows in the HadGEM2-ES
633 Earth system model using the representative concentration pathways”. *Biogeosciences* 12:
634 1317-1338
- 635 **Bian J.**, Yan R., Chen H., Lü D., Massie S.T., 2011, “Formation of the summertime ozone
636 valley over the Tibetan Plateau: The Asian summer monsoon and air column variations”.
637 *Adv. Atmos. Sci.* 28: 1318-1325
- 638 **Bowman K.W.**, Shindell D.T., Worden H.M., Lamarque J.F., Young P.J., 2013, “Evaluation
639 of ACCMIP outgoing longwave radiation from tropospheric ozone using TES satellite
640 observations”. *Atmos. Chem. Phys.* 13: 4057-4072
- 641 **Clifton O.E.**, Fiore A.M., Correa G., Horowitz L.W., Naik V., 2014, “Twenty-first century
642 reversal of the surface ozone seasonal cycle over the northeastern United States”. *Geophys.*
643 *Res. Lett.* 41: 7343-7350
- 644 **Chen X.L.**, Ma Y.M., Kelder H., Su Z., Yang K., 2011, “On the behaviour of the tropopause
645 folding events over the Tibetan Plateau”. *Atmos. Chem. Phys.* 11: 5113-5122
- 646 **Chevalier A.**, Gheusi F., Delmas R., Ordóñez C., Sarrat C., et al., 2007, “Influence of altitude
647 on ozone levels and variability in the lower troposphere: a ground-based study for Western
648 Europe over the period 2001-2004”. *Atmos. Chem. Phys.* 7: 4311-4326
- 649 **Colette A.**, Granier C., Hodnebrog Ø., Jakobs H., Maurizi A., et al., 2012, “Future air quality
650 in Europe: a multi-model assessment of projected exposure to ozone”. *Atmos. Chem. Phys.*
651 12: 10613-10630
- 652 **Cooper O.R.**, Parrish D.D., Ziemke J., Balashov N.V., Cupeiro M., 2014, “Global
653 distribution and trends of tropospheric ozone: An observation-based review”. *Elementa:*
654 *Science of the Anthropocene* 2: 000029

655 **Cooper O.R.**, Sweeney C., Gao R.S., Tarasick D., Leblanc T., 2012, “Long-term ozone
656 trends at rural ozone monitoring sites across the United States, 1990-2010”. *J. Geophys. Res.*
657 117: D22307

658 **Cubasch U.**, Wuebbles D., Chen D., Facchini M.C., Frame D., et al., 2013, “Introduction, in
659 *Climate Change 2013: The Physical Science Basis*”. Contribution of Working Group I to the
660 Fifth Assessment Report of the Intergovernmental Panel on Climate Change, edited by T. F.
661 Stocker et al., Cambridge Univ. Press, Cambridge, U. K. and New York

662 **De Marco A.**, Sicard P., Vitale M., Carriero G., Renou C., et al., 2015, “Metrics of ozone risk
663 assessment for Southern European forests: canopy moisture content as a potential plant
664 response indicator”. *Atmos. Environ.* 120: 182-190

665 **Derwent R.G.**, Utembe S.R., Jenkin M.E., Shallcross D.E., 2015, “Tropospheric ozone
666 production regions and the intercontinental origins of surface ozone over Europe”. *Atmos.*
667 *Environ.* 112: 216-224

668 **Derwent R.G.**, Manning A.J., Simmonds P.G., Spain T.G., O'Doherty S., 2013, “Analysis
669 and interpretation of 25 years of ozone observations at the Mace Head Atmospheric Research
670 Station on the Atlantic Ocean coast of Ireland from 1987 to 2012”. *Atmos. Environ.* 80: 361-
671 368

672 **Derwent R.G.**, Witham C.S., Utembe S.R., Jenkin M.E., Passant N.R., 2010, “Ozone in
673 Central England: the impact of 20 years of precursor emission controls in Europe”. *Environ.*
674 *Sci. Policy* 13: 195-204

675 **Donner L.J.**, Wyman B.L., Hemler R.S., Horowitz L.W., Ming Y., et al., 2011, “The
676 dynamical core, physical parameterizations, and basic simulation characteristics of the
677 atmospheric component AM3 of the GFDL Global Coupled Model CM3”. *J. Climate* 24:
678 3484-3519

679 **European Environment Agency**, 2015 “Air quality in Europe - 2015 report”. ISBN 978-92-
680 9213-702-1. Report No 5/2015

681 **Ellingsen K.**, Gauss M., Van Dingenen R., Dentener F.J., Emberson L., et al., 2008, “Global
682 ozone and air quality: a multi-model assessment of risks to human health and crops”. *Atmos.*
683 *Chem. Phys.* 8: 2163-2223

684 **Emberson L.D.**, Fuhrer J., Ainsworth L., Ashmore M.R., 2014, “Biodiversity and Ground-
685 level Ozone”. Report UNEP/CBD/SBSTTA/18/INF/17. Convention on Biological Diversity,
686 18th meeting, Montreal, 23-28 June 2014

687 **Fares S.**, Vargas R., Detto M., Goldstein A.H., Karlik J., et al., 2013, “Tropospheric ozone
688 reduces carbon assimilation in trees: estimates from analysis of continuous flux
689 measurements”. *Global Change Biol.* 19: 2427-2443

690 **Federal Register**, 2015, “National Ambient Air Quality Standards for Ozone”. 40 CFR Part
691 50, 51, 52, 53, and 58, pp 65292-65468

692 **Felzer B.S.F.**, Kicklighter D.W., Melillo J.M., Wang C., Zhuan Q., et al., 2004, “Ozone
693 effects on net primary production and carbon sequestration in the conterminous United States
694 using a biogeochemistry model”. *Tellus B* 56: 230-248

695 **Fiore A.M.**, Naik V., Leibensperger E.M., 2015, “Air quality and climate connections”. *J. Air*
696 *Waste Manage. Assoc.* 65: 645-685

697 **Fiore A.M.**, Naik V., Spracklen D.V., Steiner A., Unger N. et al., 2012, “Global air quality
698 and climate”. *Chem. Soc. Rev.* 41: 6663-6683

699 **Fiscus E.L.**, Booker F.L., Burkey K.O., 2005, “Crop responses to ozone: uptake, modes of
700 action, carbon assimilation and partitioning”. *Plant Cell Environ.* 28: 997-1011

701 **Gao Y.**, Fu J.S., Drake J.B., Lamarque J.F., Liu Y., 2013, “The impact of emission and
702 climate change on ozone in the United States under representative concentration pathways
703 (RCPs)”. *Atmos. Chem. Phys.* 13: 9607-9621

704 **Granier C.**, Niemeier U., Jungclaus J.H., Emmons L., Hess P., et al., 2006, “Ozone pollution
705 from future ship traffic in the Arctic northern passages”. *Geophys. Res. Lett.* 33, doi:
706 10.1029/2006GL026180

707 **Guenther A.B.**, Karl T., Harley P., Wiedinmyer C., Palmer P.I., Geron C., 2006, “Estimates
708 of global terrestrial isoprene emissions using MEGAN (Model of Emissions of Gases and
709 Aerosols from Nature)”. *Atmos. Chem. Phys.* 6: 3181-3210

710 **Guenther A.B.**, Hewitt C.N., Erickson D., Fall R., Geron, C., et al., 1995, “A global model of
711 natural volatile organic compound emissions”. *J. Geophys. Res.* 100: 8873-8892

712 **Guo D.**, Su Y., Shi C., Xunn J., Powell Jr. A.M., 2015, “Double core of ozone valley over the
713 Tibetan Plateau and its possible mechanisms”. *Journal of Atmospheric and Solar-Terrestrial*
714 *Physics* 130: 127-131

715 **Hegglin M.I.** and Shepherd T.G., 2009, “Large climate-induced changes in ultraviolet index
716 and stratosphere-to-troposphere ozone flux”. *Nature Geosci.* 2: 687

717 **Helmig D.**, Oltmans S.J., Morse T.O., Dibb J.E., 2007, “What is causing high ozone at
718 Summit, Greenland?”. *Atmos. Environ.* 41: 5031-5043

719 **Hess P.G.** and Zbinden R., 2013, “Stratospheric impact on tropospheric ozone variability and
720 trends: 1990-2009”. *Atmos. Chem. Phys.* 13: 649-674

721 **Holland M.**, Kinghorn S., Emberson L., Cinderby S., Ashmore M., et al., 2006,
722 “Development of a framework for probabilistic assessment of the economic losses caused by
723 ozone damage to crops in Europe”. UNECE International Cooperative Programme on
724 Vegetation. Contract Report EPG 1/3/205. CEH Project No: C02309NEW

725 **Hoshika Y.**, Shimizu Y., Omasa K., 2011, “A comparison between stomatal ozone uptake
726 and AOT40 of deciduous trees in Japan”. *iForest – Biogeosciences and Forestry* doi:
727 10.3832/ifor0573-004

728 **Hsu J.** and Prather M.J., 2009, “Stratospheric variability and tropospheric ozone”. *J.*
729 *Geophys. Res.* 114: D06102

730 **Hu X.M.**, Klein Petra M., Xue M. et al., 2013, “Impact of the vertical mixing induced by low-
731 level jets on boundary layer ozone concentration”. *Atmos. Environ.* 70: 123-130

732 **Hudson R.D.**, Andrade M.F., Follette M.B., Frolov A.D., 2006, “The total ozone field
733 separated into meteorological regimes – Part II: Northern Hemisphere mid-latitude total ozone
734 trends”. *Atmos. Chem. Phys.* 6: 5183-5191

735 **IPCC**, Intergovernmental Panel on Climate Change, 2014, “Summary for Policymakers”. In:
736 “Climate Change 2014: Impacts, Adaptation and Vulnerability”. Contribution of Working
737 Group II to the Fifth Assessment Report of the Intergovernmental Panel on Climate Change.
738 Cambridge University Press, Cambridge, UK

739 **Jeričević A.**, Koračin D., Jiang J., Chow J., Watson J., et al., 2013, “Air Quality Study of
740 High Ozone Levels in South California”. Part of the series NATO Science for Peace and
741 Security Series C: Environmental Security. *Air Pollution Modeling and its Application XXII:*
742 629-633

743 **Johnson C.E.**, Collins W.J., Stevenson D.S., Derwent R.G., 1999, “Relative roles of climate
744 and emissions changes on future tropospheric oxidant concentrations”. *J. Geophys. Res.* 104:
745 18631-18645

746 **Josse B.**, Simon P., Peuch V.H., 2004, “Radon global simulations with the multiscale
747 chemistry and transport model MOCAGE”. *Tellus-B* 56: 339-356

748 **Kawase H.**, Nagashima T., Sudo K., Nozawa T., 2011, “Future changes in tropospheric
749 ozone under Representative Concentration Pathways (RCPs)”. *Geophys. Res. Lett.* 38:
750 L05801

751 **Kelly J.**, Makar P.A., Plummer D.A., 2012, “Projections of mid-century summer air-quality
752 for North America: effects of changes in climate and precursor emissions”. *Atmos. Chem.*
753 *Phys.* 12: 5367-5390

754 **Kirtman B.**, Power S.B., Adedoyin J.A., Boer G.J., Bojariu R., et al., 2013, “Near-term
755 climate change: Projections and predictability, in *Climate Change 2013: The Physical Science
756 Basis*”. Contribution of Working Group I to the Fifth Assessment Report of the
757 Intergovernmental Panel on Climate Change, edited by T.F. Stocker et al., Cambridge Univ.
758 Press, Cambridge, U. K., and New York

759 **Klingberg J.**, Engardt M., Karlsson P.E., Langner J., Pleijel H., 2014, “Declining ozone
760 exposure of European vegetation under climate change and reduced precursor emissions”.
761 *Biogeosciences* 11: 5269-5283

762 **Krinner G.**, Viovy N., de Noblet-Ducoudré N., Ogée J., Polcher J., et al., 2005, “A dynamic
763 global vegetation model for studies of the coupled atmosphere-biosphere system”. *Global
764 Biogeochem. Cy.* 19: GB1015

765 **Kulkarni P.S.**, Bortoli D., Domingues A., Silva A.M., 2015, “Surface Ozone Variability and
766 Trend over Urban and Suburban Sites in Portugal”. *Aerosol Air Qual. Res.*: 1-15

767 **Kulkarni P.S.**, Bortoli D., Salgado R., Anton M., Costa M.J., et al., 2011, “Tropospheric
768 ozone variability over the Iberian Peninsula”. *Atmos. Environ.* 45: 174-182

769 **Kvalevag M.M.** and Myrhe G., 2013, “The effect of carbon-nitrogen coupling on the reduced
770 land carbon sink caused by ozone”. *Geophys. Res. Lett.* 40: 3227-3231

771 **Lamarque J.F.**, Shindell D.T., Josse B., Young P.J., Cionni I., et al., 2013, “The
772 Atmospheric Chemistry and Climate Model Intercomparison Project (ACCMIP): overview
773 and description of models, simulations and climate diagnostics”. *Geosci. Model Dev.* 6: 179-
774 206

775 **Lamarque J.F.**, Emmons L.K., Hess P.G., Kinnison D.E., Tilmes, S., et al., 2012, “CAM-
776 chem: description and evaluation of interactive atmospheric chemistry in the Community
777 Earth System Model”. *Geosci. Model Dev.* 5: 369-411

778 **Lamarque J.F.**, Bond T.C., Eyring V., Granier C., Heil A., et al., 2010, “Historical (1850–
779 2000) gridded anthropogenic and biomass burning emissions of reactive gases and aerosols:
780 methodology and application”. *Atmos. Chem. Phys.* 10: 7017-7039

781 **Lamarque J.F.**, Hess P.G., Emmons L.K., Buja L.E., Washington W.M., Granier C., 2005,
782 “Tropospheric ozone evolution between 1890 and 1990”. *J. Geophys. Res.* 110: D08304

783 **Langner J.**, Engardt M., Baklanov A., Christensen J.H., Gauss M., et al., 2012, “A multi-
784 model study of impacts of climate change on surface ozone in Europe”. *Atmos. Chem. Phys.*
785 12: 10423-10440

786 **Lau N.C.**, Leetmaa A., Nath M.J., 2006, “Attribution of atmospheric variations in the 1997-
787 2003 period to SST anomalies in the Pacific and Indian Ocean basins”. *J. Climate* 19: 3607-
788 3628

789 **Lee Y.H.** and Adams P.J., 2011, “A fast and efficient version of the two-moment aerosol
790 sectional (TOMAS) global aerosol microphysics model”. *Aerosol Sci. Tech.* 46: 678-689

791 **Lefohn A.S.**, Malley C.S., Simon H., Wells B., Xu X., et al., 2017, “Responses of human
792 health and vegetation exposure metrics to changes in ozone concentration distributions in the
793 European Union, United States, and China”. *Atmos. Environ.* 152: 123-145

794 **Lefohn A.S.**, Emery C., Shadwick D., Wernli H., Jung J., Oltmans S.J., 2014, “Estimates of
795 background surface ozone concentrations in the United States based on model-derived source
796 apportionment”. *Atmos. Environ.* 84:275-288.

797 **Lefohn A.S.**, Wernli H., Shadwick D., Oltmans S.J., Shapiro M., 2012, “Quantifying the
798 frequency of stratospheric-tropospheric transport affecting enhanced surface ozone
799 concentrations at high- and low-elevation monitoring sites in the United States”. *Atmos.*
800 *Environ.* 62: 646-656

801 **Lefohn A.S.**, Shadwick D., Oltmans S.J., 2010, “Characterizing changes in surface ozone
802 levels in metropolitan and rural areas in the United States for 1980-2008 and 1994-2008”.
803 *Atmos. Environ.* 44: 5199-5210

804 **Legrand M.**, Preunkert S., Jourdain B., Gallée H., Goutail F., et al., 2009, “Year-round record
805 of surface ozone at coastal (Dumont d’Urville) and inland (Concordia) sites in East
806 Antarctica”. *J. Geophys. Res.* 114: doi: 10.1029/2008JD011667

807 **Liu C.**, Liu Y., Cai Z., Gao S., Bian J., et al., 2010, “Dynamic formation of extreme ozone
808 minimum events over the Tibetan Plateau during northern winters 1987-2001”. *J. Geophys.*
809 *Res.* 115: D18311

810 **Meinshausen M.**, Wigley T.M.L., Raper S.C.B., 2011, “Emulating atmosphere-ocean and
811 carbon cycle models with a simpler model, MAGICC6 - Part 2: Applications”. *Atmos. Chem.*
812 *Phys.* 11: 1457-1471

813 **Mills G.**, Hayes F., Simpson D., Emberson L., Norris D., et al., 2011, “Evidence of
814 widespread effects of ozone on crops and (semi-)natural vegetation in Europe (1990-2006) in
815 relation to AOT40 and flux-based risk maps”. *Global Change Biol.* 17: 592-613

816 **Monks P.S.**, Archibald A.T., Colette A., Cooper O., Coyle M., et al., 2015, “Tropospheric
817 ozone and its precursors from the urban to the global scale from air quality to short-lived
818 climate forcer”. *Atmos. Chem. Phys.* 15: 8889-8973

819 **Moura B.B.**, Alves E.S., de Souza S.R., Domingos M., Vollenweider P., 2014, “Ozone
820 phytotoxic potential with regard to fragments of the Atlantic Semi-deciduous Forest
821 downwind of Sao Paulo, Brazil”. *Environ. Pollut.* 192: 65-73

822 **Myhre G.**, Shindell D., Bréon F.M., Collins W., Fuglestedt J., et al., 2013, “Anthropogenic
823 and Natural Radiative Forcing”. In: *Climate Change 2013: The Physical Science Basis.*
824 *Contribution of Working Group I to the Fifth Assessment Report of the Intergovernmental*
825 *Panel on Climate Change.* Cambridge University Press, Cambridge, United Kingdom and
826 New York, USA

827 **Naik V.**, Voulgarakis A., Fiore A.M., Horowitz L.W., Lamarque J.F., et al., 2012,
828 “Preindustrial to present day changes in tropospheric hydroxyl radical and methane lifetime
829 from the Atmospheric Chemistry and Climate Model Intercomparison Project (ACCMIP)”.
830 *Atmos. Chem. Phys. Discuss.* 12: 30755-30804

831 **Nazarenko L.**, Schmidt G.A., Miller R.L., Tausnev N., Kelley M., et al., 2015, “Future
832 climate change under RCP emission scenarios with GISS ModelE2”. *J. Adv. Model. Earth*
833 *Syst.* 7: 244-267

834 **Nemani R.R.**, Keeling C.D., Hashimoto H., Jolly W.M., Piper S.C., et al., 2003, “Climate-
835 Driven Increases in Global Terrestrial Net Primary Production from 1982 to 1999”. *Science*
836 300: 1560-1563

837 **Ollinger S.V.**, Aber J.D., Reich P.B., 1997, “Simulating ozone effects on forest productivity:
838 interactions among leaf, canopy, and stand-level processes”. *Ecol. Appl.* 7: 1237-1251.

839 **Oltmans S.J.**, Lefohn A.S., Harris J.M., Galbally I., Scheel H.E., et al., 2006, “Long-term
840 changes in tropospheric ozone”. *Atmos. Environ.* 40: 3156-3173

841 **Paoletti E.**, De Marco A., Beddows D.C.S., Harrison R.M., Manning W.J., 2014, “Ozone
842 levels in European and USA cities are increasing more than at rural sites, while peak values
843 are decreasing”. *Environ. Pollut.* 192: 295-299

844 **Paoletti E.** and Manning W.J., 2007, “Toward a biologically significant and usable standard
845 for ozone that will also protect plants”. *Environ. Pollut.* 150: 85-95

846 **Paoletti E.**, 2006, “Impact of ozone on Mediterranean forest: A review”. *Environ. Pollut.* 144:
847 463-474

848 **Parrish D.D.**, Law K.S., Staehelin J., Derwent R., Cooper O.R., et al., 2012, “Long-term
849 changes in lower tropospheric baseline ozone concentrations at northern mid-latitudes”.
850 *Atmos. Chem. Phys.* 12: 11485-11504

851 **Pfister G.G.**, Walters S., Lamarque J.F., Fast J., Barth M.C., et al., 2014, “Projections of
852 future summertime ozone over the U.S”. *J. Geophys. Res. Atmos.* 119: 5559-5582

853 **Price C.** and Rind D.H., 1992, "A simple lightning parameterization for calculating global
854 lightning distributions". *J. Geophys. Res.*, 97: 9919-9933

855 **Proietti C.**, Anav A., De Marco A., Sicard P., Vitale M., 2016, "A multi-sites analysis on the
856 ozone effects on Gross Primary Production of European forests". *Sci. Total Environ.* 556: 1-
857 11

858 **Querol X.**, Alastuey A., Pandolfi M., Reche C., Pérez N., et al., 2014, "2001-2012 trends on
859 air quality in Spain". *Sci. Total Environ.* 490: 957-969.

860 **Reich P.B.**, 1987, "Quantifying plant response to ozone: a unifying theory". *Tree Physiol.* 3:
861 63-91

862 **Ren W.**, Tian H., Liu M., Zhang C., Chen G., et al., 2007, "Effects of tropospheric ozone
863 pollution on net primary productivity and carbon storage in terrestrial ecosystems of China".
864 *J. Geophys. Res.* 112: 1-17

865 **Riahi K.**, Rao S., Krey V., Cho C., Chirkov V., et al., 2011, "RCP 8.5 - A scenario of
866 comparatively high greenhouse gas emissions". *Climatic Change* 109: 33-57

867 **Rieder H.E.**, Fiore A.M., Horowitz L.W., Naik V., 2015, "Projecting policy-relevant metrics
868 for high summertime ozone pollution events over the eastern United States due to climate and
869 emission changes during the 21st century". *J. Geophys. Res. Atmos.* 120: 784-800

870 **Ridley B.A.**, Pickering K.E., Dye, J.E., 2005, "Comments on the parameterization of
871 lightning-produced NO in global chemistry-transport models". *Atmos. Environ.* 39: 6184-
872 6187

873 **Ochoa-Hueso R.**, Munzi S., Alonso R., Sicard P., Stevens C. et al., 2017, "Ecological
874 Impacts of Atmospheric Pollution and Interactions with Climate Change in Terrestrial
875 Ecosystems of the Mediterranean Basin: Current Research and Future Directions". *Environ.*
876 *Pollut.* 227: 194-206

877 **Sanderson M.G.**, Collins W.J., Hemming D.L., Betts R.A., 2007, "Stomatal conductance
878 changes due to increasing carbon dioxide levels: Projected impact on surface ozone levels".
879 *Tellus* 59B: 404-411

880 **Sanderson M.G.**, Jones C.D., Collins W.J., Johnson C.E., Derwent R.G., 2003, "Effect of
881 climate change on isoprene emissions and surface ozone levels". *Geophys. Res. Lett.* 30: 1936

882 **Schnell J.L.**, Prather M.J., Josse B., Naik V., Horowitz L.W., et al., 2016, "Effect of climate
883 change on surface ozone over North America, Europe, and East Asia". *Geophys. Res. Lett.* 43:
884 L068060

885 **Seidel D.J.**, Fu Q., Randel W.J., Reichler T.J., 2008, "Widening of the tropical belt in a
886 changing climate". *Nat. Geosci* 1: 21-4

887 **Shindell D.T.**, Lamarque J.F., Schulz M., Flanner M., Jiao C., et al., 2012, "Radiative forcing
888 in the ACCMIP historical and future climate simulations". *Atmos. Chem. Phys. Discuss.* 12:
889 21105-21210

890 **Shindell D.T.**, Faluvegi G., Stevenson D.S., Krol M.C., Emmons L.K., et al., 2006, "Multi-
891 model simulations of carbon monoxide: Comparison with observations and projected near-
892 future changes". *J. Geophys. Res.* 111: D19306

893 **Sicard P.**, Serra R., Rossello P., 2016a, "Spatiotemporal trends of surface ozone
894 concentrations and metrics in France". *Environ. Res.* 149: 122-144

895 **Sicard P.**, Augustaitis A., Belyazid S., Calfapietra C., De Marco A., et al., 2016b, "Global
896 topics and novel approaches in the study of air pollution, climate change and forest
897 ecosystems". *Environ. Pollut.* 213: 977-987

898 **Sicard P.**, De Marco A., Dalstein-Richier L., Tagliaferro F., Paoletti E., 2016c, "An
899 epidemiological assessment of stomatal ozone flux-based critical levels for visible ozone
900 injury in Southern European forests". *Sci. Total Environ.* 541: 729-741

901 **Sicard P.**, De Marco A., Troussier F., Renou C., Vas N., Paoletti E., 2013, “Decrease in
902 surface ozone concentrations at Mediterranean remote sites and increase in the cities”. *Atmos.*
903 *Environ.* 79: 705-715

904 **Sicard P.**, Vas N., Dalstein-Richier L., 2011, “Annual and seasonal trends for ambient ozone
905 concentration and its Impact on Forest Vegetation in Mercantour National Park (South-eastern
906 France) over the 2000-2008 period”. *Environ. Pollut.* 159: 351-362

907 **Sicard P.**, Coddeville P., Galloo J.C., 2009, “Near-surface ozone levels and trends at rural
908 stations in France over the 1995-2003 period”. *Environ. Monit. Assess.* 156: 141-157

909 **Simpson D.**, Arneth A., Mills G., Solberg S., Uddling J., 2014, “Ozone - the persistent
910 menace: interactions with the N cycle and climate change”. *Curr. Opin. Env. Sust.* 9-10: 9-19

911 **Singh H.B.**, Herlth D., O'Hara D., Zahnle K., Bradshaw J.D., et al., 1992, “Relationship of
912 Peroxyacetyl nitrate to active and total odd nitrogen at northern high latitudes: influence of
913 reservoir species on NO_x and O₃”. *J. Geophys. Res.* 97:16523-30

914 **Sitch S.**, Cox P.M., Collins W.J., Huntingford C., 2007, “Indirect radiative forcing of climate
915 change through ozone effects on the land-carbon sink”. *Nature* 448: 791-794

916 **Steinbacher M.**, Henne S., Dommen J., Wiesen P., Prevot A.S.H., 2004, “Nocturnal trans-
917 alpine transport of ozone and its effects on air quality on the Swiss Plateau”. *Atmos. Environ.*
918 38: 4539-4550

919 **Stevenson D.S.**, Young P.J., Naik V., Lamarque J.F., Shindell D.T., et al., 2013,
920 “Tropospheric ozone changes, radiative forcing and attribution to emissions in the
921 Atmospheric Chemistry and Climate Model Inter-comparison Project (ACCMIP)”. *Atmos.*
922 *Chem. Phys.* 13: 3063-3085

923 **Stevenson D.S.**, Young P.J., Naik V., Lamarque J.F., Shindell D.T., et al., 2012,
924 “Tropospheric ozone changes, radiative forcing and attribution to emissions in the
925 Atmospheric Chemistry and Climate Model Inter-comparison Project (ACCMIP)”. *Atmos.*
926 *Chem. Phys. Discuss.* 12: 26047-26097

927 **Stevenson D.S.**, Dentener F.J., Schultz M.G., Ellingsen K., van Noije T.P.C., et al., 2006,
928 “Multi-model ensemble simulations of present-day and near-future tropospheric ozone”. *J.*
929 *Geophys. Res.* 111: D08301

930 **Stevenson D.S.**, Johnson C.E., Collins W.J., Derwent R.G., Edwards J.M., 2000, “Future
931 estimates of tropospheric ozone radiative forcing and methane turnover – The impact of
932 climate change”. *Geophys. Res. Lett.* 27: 2073-2076

933 **Stohl A.**, Berg T., Burkhardt J.F., Fjaeraa A.M., Forster C., et al., 2007, « Arctic smoke -
934 record high air pollution levels in the European Arctic due to agricultural fires in Eastern
935 Europe in spring 2006”. *Atmos. Chem. Phys.* 7: 511-534

936 **Tang Q.**, Prather M.J., Hsu J., 2011, “Stratosphere-troposphere exchange ozone flux related
937 to deep convection”. *Geophys. Res. Lett.* 38: L03806

938 **Teyssèdre H.**, Michou M., Clark H.L., Josse B., Karcher F., et al., 2007, “A new tropospheric
939 and stratospheric Chemistry and Transport Model MOCAGE-Climat for multi-year studies:
940 evaluation of the present-day climatology and sensitivity to surface processes”. *Atmos. Chem.*
941 *Phys.* 7: 5815-5860

942 **Tian W.**, Chipperfield M., Huang Q., 2008, “Effects of the Tibetan Plateau on total column
943 ozone distribution”. *Tellus* 60B: 622-635

944 **UNECE**, United Nations Economic Commission for Europe. Convention on Long-Range
945 Trans-boundary Air Pollution, 2010, “Mapping Critical Levels for Vegetation”. International
946 Cooperative Programme on Effects of Air Pollution on Natural Vegetation and Crops,
947 Bangor, UK

948 **van Vuuren D.**, Edmonds J., Kainuma M., Riahi K., Thomson A., et al., 2011, “The
949 representative concentration pathways: an overview”. *Climatic Change* 109: 5-31

950 **Voulgarakis A.**, Naik V., Lamarque J.F., Shindell D.T., Young P.J. et al., 2013, “Analysis of
951 present day and future OH and methane lifetime in the ACCMIP simulations”. *Atmos. Chem.*
952 *Phys.* 13: 2563-2587

953 **Walker T.W.**, Jones D.B.A., Parrington M., Henze D.K., Murray L.T., et al., 2012, “Impacts
954 of mid-latitude precursor emissions and local photochemistry on ozone abundances in the
955 Arctic”. *Journal of Geophysical Research: Atmospheres* 117, doi: 10.1029/2011JD016370

956 **Wang Q.Y.**, Gao R.S., Cao J.J., Schwarz J.P., Fahey D.W., et al. 2015, “Observations of high
957 level of ozone at Qinghai Lake basin in the northeastern Qinghai-Tibetan Plateau, western
958 China”. *J. Atm. Chem.* 72: 19-26

959 **Wang X.** and Mauzerall D.L., 2004, “Characterizing distributions of surface ozone and its
960 impact on grain production in China, Japan and South Korea: 1900 and 2020”. *Atmos.*
961 *Environ.* 38: 4383-4402

962 **Watanabe S.**, Hajima T., Sudo K., Nagashima T., Takemura T., et al., 2011, “MIROC-ESM
963 2010: model description and basic results of CMIP5-20c3m experiments”. *Geosci. Model*
964 *Dev.* 4: 845-872

965 **Wesely M.L.** and Hicks B.B., 2000, “A review of the current status of knowledge in dry
966 deposition”. *Atmos. Environ.* 34: 2261-2282

967 **Wild O.**, Fiore A.M., Shindell D.T., Doherty R.M., Collins W.J., et al., 2012, “Modelling
968 future changes in surface ozone: a parameterized approach”. *Atmos. Chem. Phys.* 12: 2037-
969 2054

970 **Wild O.**, 2007, “Modelling the global tropospheric ozone budget: exploring the variability in
971 current models”. *Atmos. Chem. Phys.* 7: 2643-2660

972 **Williams E.R.**, 2009, “The global electrical circuit: A review”. *Atmos. Res.*, 91: 140-152.

973 **Wilson R.C.**, Fleming Z. L., Monks P. S., Clain G., Henne S., et al., 2012, “Have primary
974 emission reduction measures reduced ozone across Europe? An analysis of European rural
975 background ozone trends 1996-2005”. *Atmos. Chem. Phys.* 12: 437-454

976 **Wittig V.E.**, Ainsworth E.A., Naidu S.L., Karnosky D.F., Long S.P., 2009, “Quantifying the
977 impact of current and future tropospheric ozone on tree biomass, growth, physiology and
978 biochemistry: a quantitative meta-analysis”. *Global Change Biol.* 15: 396-424

979 **Wittig V.E.**, Ainsworth E.A., Long S.P., 2007, “To what extent do current and projected
980 increases in surface ozone affect photosynthesis and stomatal conductance of trees? A meta-
981 analytic review of the last 3 decades of experiments”. *Plant, Cell Environ.* 30: 1150-1162

982 **Xing J.**, Mathur R., Pleim J., C. Hogrefe, Gan C.M., et al., 2015, “Observations and modeling
983 of air quality trends over 1990–2010 across the Northern Hemisphere: China, the United
984 States and Europe”. *Atmos. Chem. Phys.* 15: 2723-2747

985 **Young P.J.**, Archibald A.T., Bowman K.W., Lamarque J.F., Naik V., et al., 2013,
986 “Preindustrial to end 21st century projections of tropospheric ozone from the Atmospheric
987 Chemistry and Climate Model Intercomparison Project (ACCMIP)”. *Atmos. Chem. Phys.* 13:
988 2063-2090

989 **Zak D.R.**, Pregitzer K.S., Kubiske M.E., Burton A.J., 2011, “Forest productivity under
990 elevated CO₂ and O₃; positive feedbacks to soil N cycling sustain decade-long net primary
991 productivity enhancement by CO₂. *Ecology Letters* 14: 1220-1226

992 **Zeng G.**, Morgenstern O., Braesicke P., Pyle J.A., 2010, “Impact of stratospheric ozone
993 recovery on tropospheric ozone and its budget”. *Geophys. Res. Lett.* 37: L09805

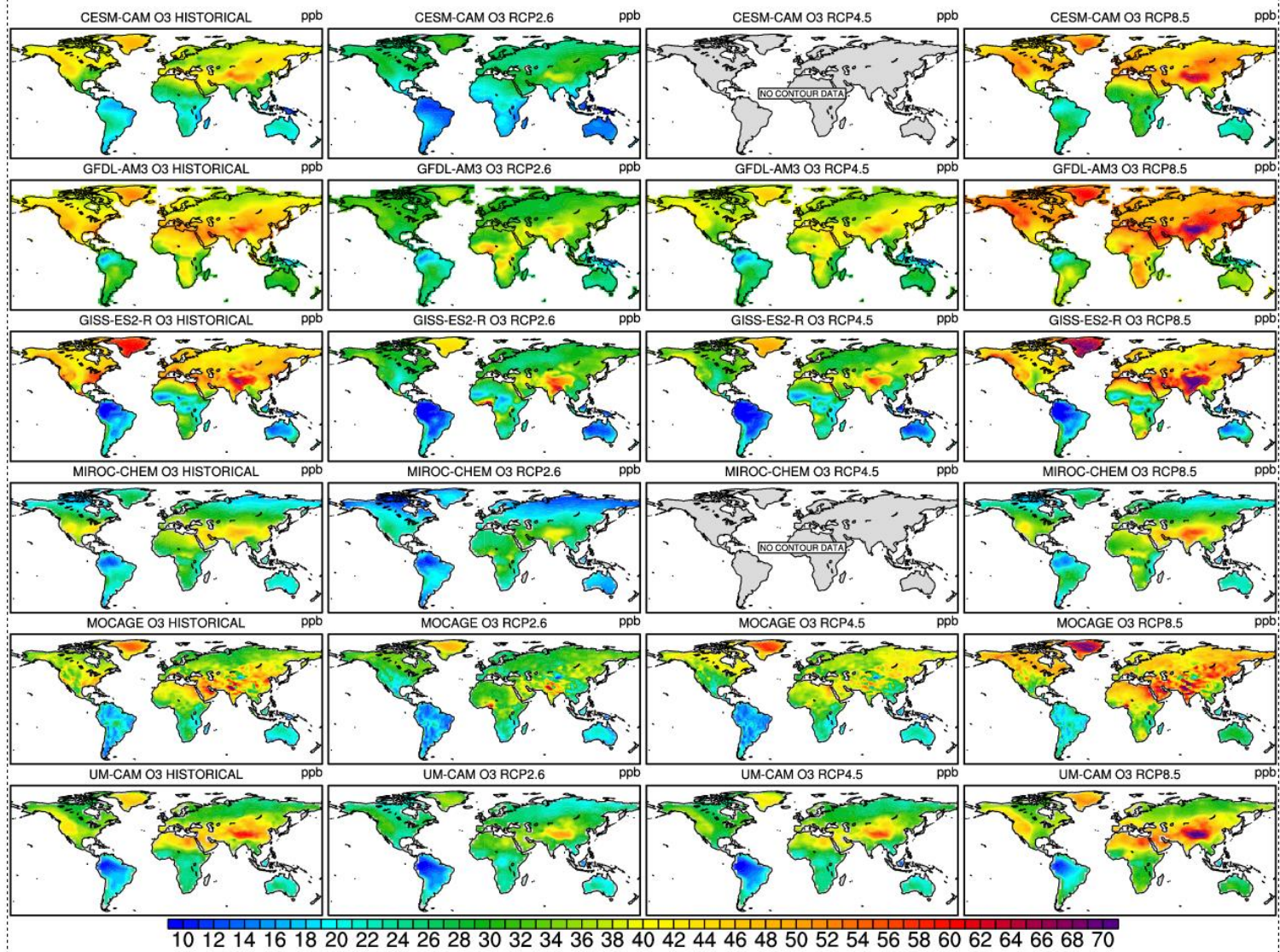
994 **Zeng G.**, Pyle J.A., Young P. J., 2008, “Impact of climate change on tropospheric ozone and
995 its global budgets, *Atmos. Chem. Phys.* 8: 369-387

996 **Zeng G.** and Pyle J.A., 2003, “Changes in tropospheric ozone between 2000 and 2100
997 modeled in a chemistry-climate model”. *Geophys. Res. Lett.* 30: 1392

998 **Zhang Q.**, Streets D.G., Carmichael G.R., He K.B., Huo H., et al., 2009, “Asian emissions in
999 2006 for the NASA INTEX-B mission”. *Atmos. Chem. Phys.* 9: 5131-5153

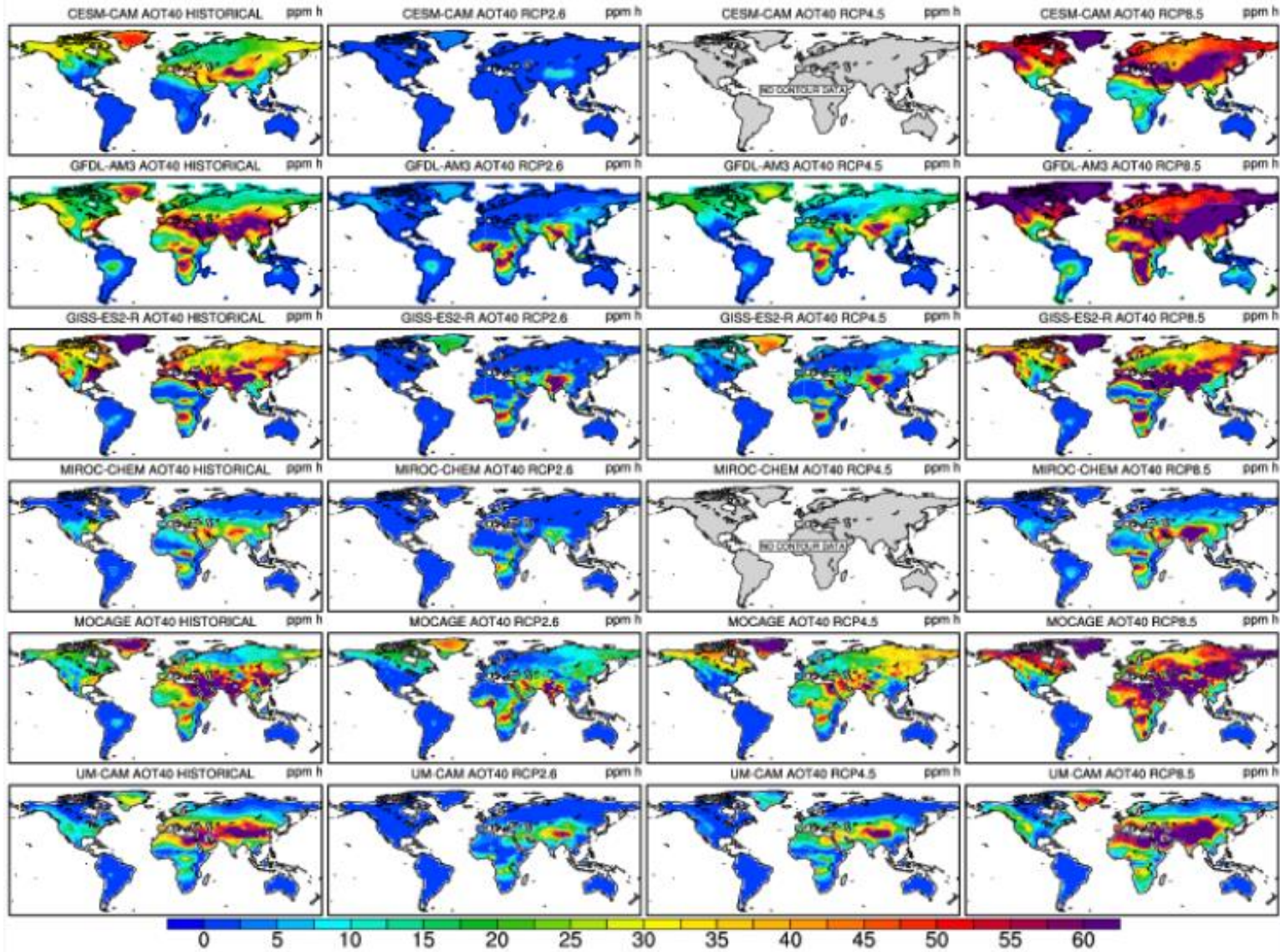
1000 **Zhang M.**, Xu Y., Uno I., Akimoto H., 2004, "A numerical study of tropospheric ozone in the
1001 springtime in east Asia". *Adv. Atmos. Sci.* 21: 163-170
1002 **Zhang L.**, Brook J. R., Vet R., 2003, "A revised parameterization for gaseous dry deposition
1003 in air-quality models". *Atmos. Chem. Phys.* 3: 2067-2082
1004 **Zhu Z.**, Piao S., Myneni R.B., Huang M., Zeng Z., et al., 2016, "Greening of the Earth and its
1005 drivers". *Nature Climate Change* 6: 791-795
1006
1007
1008
1009

1010 **Figure 1:** Surface ozone average concentrations (in ppb) at the lower model layer for each ACCMIP model over the historical
1011 period and for RCP2.6, RCP4.5 and RCP8.5 simulations by 2100. The data are missing for 2 models under RCP4.5 ("No contour
1012 data").



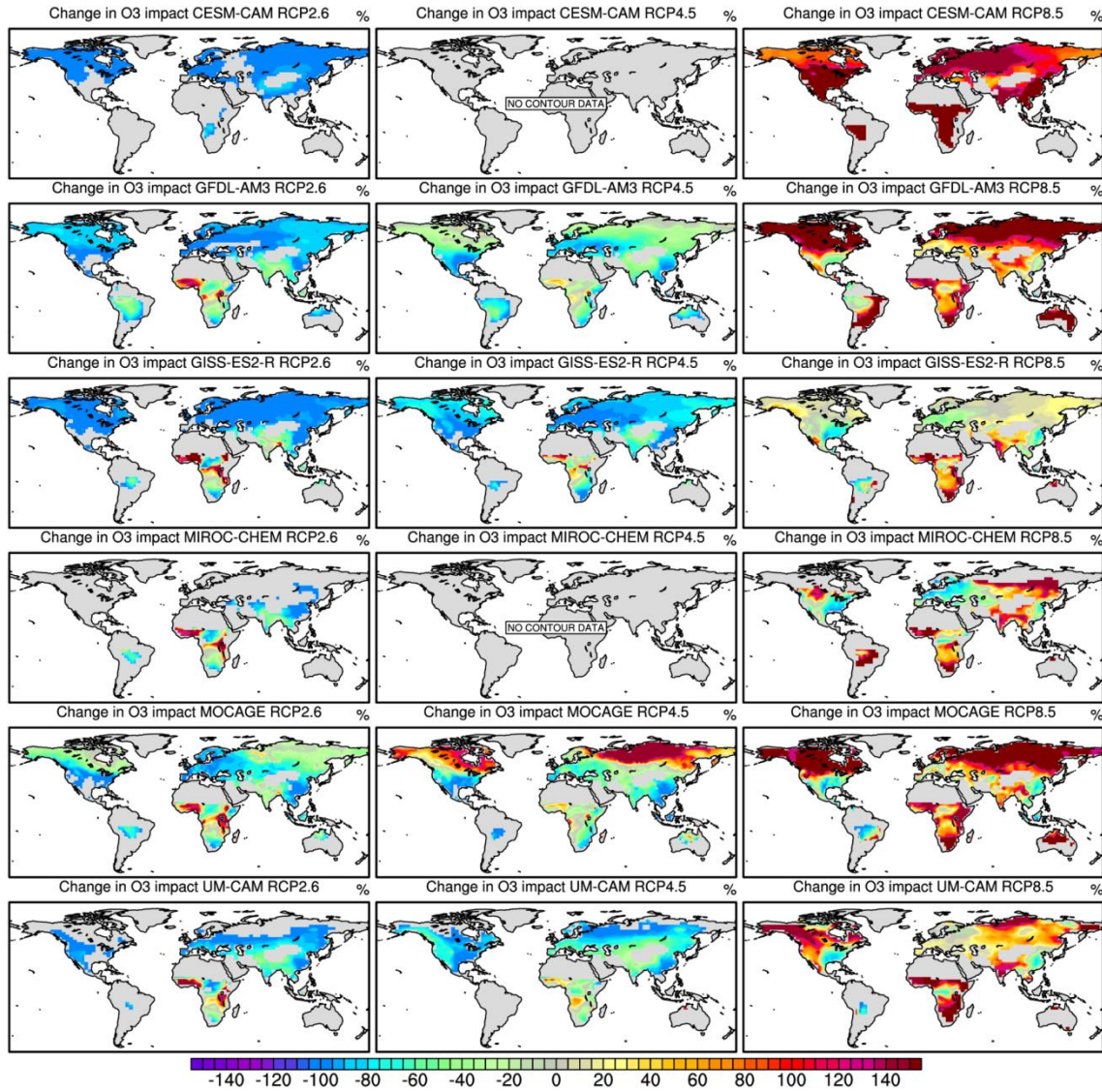
1013
1014

1015 **Figure 2:** Surface mean AOT40 (in ppm.h) at the lower model layer for each ACCMIP model over the historical period and for
 1016 RCP2.6, RCP4.5 and RCP8.5 simulations by 2100. The data are missing for 2 models under RCP4.5 ("No contour data").



1017

1018 **Figure 3:** Simulated percentage changes (%) in the potential ozone impact on photosynthetic carbon assimilation (IO3) for each
1019 ACCMIP model between RCP2.6, RCP4.5 and RCP8.5 simulations and the historical run. The data are missing for 2 models under
1020 RCP4.5 ("No contour data").



1022 **Table 1:** Characteristics of the models, including simulation time slice, spatial resolution, simulated gas species and associated
 1023 bibliographic references (from Lamarque et al., 2013 and Young et al. 2013). Black carbon (BC), Organic carbon (OC), Secondary
 1024 Organic Aerosols (SOA), Dimethylsulfide (DMS), Chemistry Climate Model (CCM), Chemistry Transport Model (CTM),
 1025 Chemistry-General Circulation Model (CGCM).
 1026

| Models | Type | Simulation length | Resolution (lat/lon) | Number of vertical pressure levels & top level | Species simulated | References |
|------------|------|-------------------------|----------------------|--|--|--|
| CESM-CAM | CCM | 2000-2009 and 2100-2109 | 1.875/2.5 | 26 levels 3.5 hPa | 16 gas species; constant present-day isoprene, soil NO _x , DMS and volcanic sulfur, oceanic CO. | Lamarque et al., 2012 |
| GFDL-AM3 | CCM | 2001-2010 and 2101-2110 | 2.0/2.5 | 48 levels 0.017 hPa | 81 gas species; SO _x , BC, OC, SOA, NH ₃ , NO ₃ ; constant pre-industrial soil NO _x ; constant present-day soil and oceanic CO, and biogenic VOC; climate-sensitive dust, sea salt, and DMS. | Donner et al., 2011 Naik et al., 2012 |
| GISS-E2-R | CCM | 2000-2004 and 2101-2105 | 2.0/2.5 | 40 levels 0.14 hPa | 51 gas species; interactive sulfate, BC, OC, sea salt, dust, NO ₃ , SOA, alkenes; constant present-day soil NO _x ; climate-sensitive dust, sea salt, and DMS; climate-sensitive isoprene based on present-day vegetation. | Lee and Adams, 2011 Shindell et al., 2012 |
| MIROC-CHEM | CCM | 2000-2010 and 2100-2104 | 2.8/2.8 | 80 levels 0.003 hPa | 58 gas species; SO ₄ , BC, OC; constant present-day VOCs, soil-NO _x , oceanic-CO; climate-sensitive dust, sea salt and DMS. | Watanabe et al., 2011 |
| MOCAGE | CTM | 2000-2003 and 2100-2103 | 2.0/2.0 | 47 levels 6.9 hPa | 110 gas species; constant present-day isoprene, other VOCs, oceanic CO and soil NO _x . | Josse et al., 2004 Krinner et al., 2005 Teyssèdre et al., 2007 |
| UM-CAM | CGCM | 2000-2005 and 2094-2099 | 2.50/3.75 | 19 levels 4.6 hPa | 60 gas species; constant present-day biogenic isoprene, soil NO _x , biogenic and oceanic CO. | Zeng et al., 2008, 2010 |

1027

1028 **Table 2a:** Annual total emissions of CO (Tg CO/year), NMVOCs (Tg C/year), NO_x (Tg N/year, including lightning and soil NO_x),
 1029 total lightning NO_x emissions (LNO_x) and global atmospheric methane (CH₄) burden (Tg) for the historical simulations in each
 1030 model (from Young et al., 2013 and * from Voulgarakis et al., 2013).
 1031

| Models | Historical | | | | |
|------------|------------|-------------------|--------|-----------------|-------------------|
| | CO | * CH ₄ | NMVOCs | NO _x | *LNO _x |
| CESM-CAM | 1248 | 4902 | 429 | 50.0 | 4.2 |
| GFDL-AM3 | 1246 | 4809 | 830 | 46.2 | 4.4 |
| GISS-E2-R | 1070 | 4793 | 830 | 48.6 | 7.7 |
| MIROC-CHEM | 1064 | 4805 | 833 | 57.3 | 9.7 |
| MOCAGE | 1168 | 4678 | 1059 | 47.9 | 5.2 |
| UM-CAM | 1148 | 4879 | 535 | 49.2 | 5.1 |

1033
 1034
 1035

1036
 1037
 1038
 1039
 1040
 1041

1042 **Table 2b:** Simulated percentage (%) changes in total emissions of CO, NMVOCs, NO_x (including lightning and soil NO_x), total
 1043 lightning NO_x emissions (LNO_x) and global atmospheric CH₄ burden for each model between 2100 and historical simulation for
 1044 RCPs (from Young et al., 2013 and *Voulgarakis et al., 2013). The last row shows means and standard deviations (SD). Missing or
 1045 not available data are identified (n.a).
 1046

| Models | RCP2.6 scenario | | | | | RCP4.5 scenario | | | | | RCP8.5 scenario | | | | |
|------------|-----------------|----------------|-----------------|-------------------|------------------|-----------------|-----------------|-----------------|-------------------|------------------|-----------------|-----------------|-----------------|-------------------|-------------------|
| | CO | VOCs | NO _x | *LNO _x | *CH ₄ | CO | VOCs | NO _x | *LNO _x | *CH ₄ | CO | VOCs | NO _x | *LNO _x | *CH ₄ |
| CESM-CAM | - 36.7 | 0 | - 52.8 | + 7.1 | - 27.1 | n.a | n.a | n.a | n.a | n.a | - 30.1 | 0 | - 33.0 | + 29.7 | + 112.1 |
| GFDL-AM3 | - 36.9 | - 5.0 | - 47.0 | + 12.6 | - 27.9 | - 47.4 | - 3.6 | - 41.5 | + 23.5 | - 9.3 | - 30.3 | - 1.9 | - 22.4 | + 38.2 | + 116.1 |
| GISS-E2-R | - 42.8 | + 0.5 | - 44.2 | + 3.8 | - 21.0 | - 54.9 | + 6.9 | - 39.2 | + 12.2 | + 4.6 | - 35.1 | + 19.8 | - 20.0 | + 26.2 | + 152.7 |
| MIROC-CHEM | - 43.1 | - 7.1 | - 36.0 | + 7.5 | - 28.2 | n.a | n.a | n.a | n.a | n.a | - 35.4 | - 3.4 | - 6.9 | + 38.0 | + 116.0 |
| MOCAGE | - 39.4 | - 6.5 | - 45.7 | + 5.2 | - 28.8 | n.a | n.a | n.a | n.a | n.a | - 32.3 | - 2.8 | - 22.9 | + 19.9 | + 113.4 |
| UM-CAM | - 39.0 | - 11.3 | - 40.6 | + 8.1 | - 27.9 | - 50.4 | - 9.2 | - 36.0 | + 17.5 | - 8.7 | - 32.0 | - 4.2 | - 17.2 | + 43.6 | + 112.1 |
| Mean ± SD | - 39.7 ± 2.2 | - 4.9 ± 4.9 | - 44.4 ± 4.3 | + 7.4 ± 2.0 | - 26.8 ± 3.7 | - 50.9 ± 3.2 | - 2.0 ± 11.4 | - 38.9 ± 2.3 | + 17.7 ± 3.7 | - 4.5 ± 9.4 | - 32.5 ± 1.8 | + 1.3 ± 11.6 | - 20.4 ± 7.0 | + 32.6 ± 10.8 | + 120.4 ± 19.5 |

1047
 1048

1049 **Table 3a:** Global and hemispheric (averaged over the land points of the domain) mean annual-average surface ozone concentrations
 1050 (in ppb) and mean AOT40 (in ppm.h) for the historical simulations in each model (North and South Hemisphere, i.e NH and SH).
 1051 The last row shows means and standard deviations (SD).
 1052

| Models | Ozone conc. global | Ozone conc. SH | Ozone conc. NH | AOT40 global | AOT40 SH | AOT40 NH |
|---------------|-----------------------|-------------------|-------------------|-----------------|---------------|-----------------|
| CESM-CAM | 31.3 | 20.9 | 36.4 | 12.8 | 0.2 | 18.9 |
| GFDL-AM3 | 38.6 | 30.6 | 42.9 | 21.8 | 4.7 | 30.8 |
| GISS-E2-R | 35.8 | 22.3 | 42.3 | 26.0 | 3.6 | 36.8 |
| MIROC-CHEM | 27.9 | 20.4 | 31.4 | 7.3 | 1.9 | 9.8 |
| MOCAGE | 32.9 | 21.5 | 38.3 | 22.9 | 3.5 | 31.8 |
| UM-CAM | 31.3 | 21.4 | 36.0 | 14.4 | 1.3 | 20.6 |
| Mean \pm SD | 33.0 \pm 3.8 | 22.9 \pm 3.8 | 37.9 \pm 4.3 | 17.5 \pm 7.2 | 2.5 \pm 1.7 | 24.8 \pm 10.1 |

1053
 1054
 1055
 1056
 1057
 1058
 1059
 1060

Table 3b: Simulated percentage (%) changes in global and hemispheric mean annual-average surface ozone concentrations (over the land points of the domain) and in global mean stratospheric ozone column (* from Voulgarakis et al., 2013) for each model between 2100 and historical simulation for RCPs (North and South Hemisphere, i.e NH and SH). The last row shows means and standard deviations (SD). Missing or not available data are identified (n.a).

| Models | Surface ozone mean concentrations | | | | | | | | | * Stratospheric ozone | | |
|---------------|-----------------------------------|-----------------|------------------|------------------|------------------|------------------|------------------|-------------------|------------------|-----------------------|------------------|------------------|
| | RCP2.6 global | RCP2.6 SH | RCP2.6 NH | RCP4.5 global | RCP4.5 SH | RCP4.5 NH | RCP8.5 global | RCP8.5 SH | RCP8.5 NH | RCP2.6 global | RCP4.5 global | RCP8.5 global |
| CESM-CAM | - 29.1 | - 20.6 | - 31.3 | n.a | n.a | n.a | + 21.9 | + 22.5 | + 20.5 | n.a | n.a | + 5.3 |
| GFDL-AM3 | - 20.5 | - 10.8 | - 24.5 | - 11.7 | - 6.9 | - 13.5 | + 15.5 | + 18.6 | + 14.5 | + 3.3 | + 3.9 | + 8.4 |
| GISS-E2-R | - 23.5 | - 5.8 | - 27.9 | - 20.4 | - 6.3 | - 23.9 | + 7.0 | + 19.3 | + 3.8 | + 8.0 | + 8.8 | + 15.1 |
| MIROC-CHEM | - 23.3 | - 12.3 | - 26.8 | n.a | n.a | n.a | + 3.9 | + 10.3 | + 2.2 | + 2.6 | n.a | + 4.2 |
| MOCAGE | - 12.8 | + 7.4 | - 18.5 | - 1.8 | + 17.7 | - 7.0 | + 23.1 | + 40.4 | + 16.7 | + 19.9 | n.a | + 23.6 |
| UM-CAM | - 17.3 | - 4.7 | - 21.1 | - 8.3 | + 0.9 | - 10.8 | + 14.4 | + 24.3 | + 11.4 | + 6.7 | + 6.9 | + 7.4 |
| Mean \pm SD | - 21.1 \pm 5.6 | - 7.8 \pm 9.4 | - 25.0 \pm 4.7 | - 10.5 \pm 7.7 | + 1.4 \pm 11.5 | - 13.8 \pm 7.2 | + 13.8 \pm 7.1 | + 22.6 \pm 10.0 | + 11.5 \pm 7.3 | + 8.1 \pm 7.0 | + 6.5 \pm 2.5 | + 10.7 \pm 7.4 |

1061
 1062

1063 **Table 3c:** Simulated percentage (%) changes in global and hemispheric mean AOT40 (over the land points of the domain) for each
 1064 model between 2100 and historical simulation for RCPs (North and South Hemisphere, i.e NH and SH). Missing or not available
 1065 data are identified (n.a).
 1066

| Models | AOT40 | | | | | | | | |
|------------|---------------|--------------|---------------|---------------|----------------|---------------|---------------|-----------------|---------------|
| | RCP2.6 global | RCP2.6 SH | RCP2.6 NH | RCP4.5 global | RCP4.5 SH | RCP4.5 NH | RCP8.5 global | RCP8.5 SH | RCP8.5 NH |
| CESM-CAM | - 96.9 | - 99.9 | - 96.8 | n.a | n.a | n.a | + 138.3 | + 150.0 | + 134.9 |
| GFDL-AM3 | - 75.2 | - 25.5 | - 78.9 | - 53.2 | - 36.2 | - 54.5 | + 96.3 | + 242.5 | + 85.1 |
| GISS-E2-R | - 78.1 | - 13.9 | - 81.2 | - 75.0 | - 27.8 | - 77.2 | + 22.3 | + 83.3 | + 19.5 |
| MIROC-CHEM | - 74.0 | - 10.5 | - 80.6 | n.a | n.a | n.a | + 20.5 | + 78.9 | + 16.3 |
| MOCAGE | - 53.7 | + 68.6 | - 59.7 | - 17.5 | + 202.9 | - 28.3 | + 85.1 | + 448.6 | + 67.0 |
| UM-CAM | - 73.6 | + 92.3 | - 76.7 | - 52.8 | +7.7 | - 54.8 | + 49.3 | + 176.9 | + 45.1 |
| Mean ± SD | - 75.2 ± 13.7 | + 1.9 ± 69.5 | - 79.0 ± 11.8 | - 49.6 ± 23.8 | + 36.6 ± 112.4 | - 53.7 ± 20.0 | + 68.6 ± 46.3 | + 196.7 ± 137.7 | + 61.3 ± 44.8 |

1067
 1068 **Table 3d:** Simulated percentage (%) changes in potential O₃ impact on vegetation (IO3, over the land points of the domain) for each
 1069 model between 2100 and historical simulation for RCPs (North and South Hemisphere, i.e NH and SH).Missing or not available
 1070 data are identified (n.a).
 1071
 1072

| Models | Risk factor IO3 | | | | | | | | |
|------------|-----------------|---------------|---------------|---------------|---------------|---------------|---------------|---------------|---------------|
| | RCP2.6 global | RCP2.6 SH | RCP2.6 NH | RCP4.5 global | RCP4.5 SH | RCP4.5 NH | RCP8.5 global | RCP8.5 SH | RCP8.5 NH |
| CESM-CAM | - 97.2 | - 91.8 | -97.5 | n.a | n.a | n.a | + 129.6 | +146.8 | +127.5 |
| GFDL-AM3 | - 69.4 | - 49.1 | - 74.8 | - 50.1 | - 61.1 | - 47.2 | + 91.9 | +95.5 | +90.4 |
| GISS-E2-R | - 66.1 | - 20.7 | - 74.3 | - 71.7 | - 53.3 | - 74.6 | + 21.5 | +56.6 | +14.2 |
| MIROC-CHEM | - 41.4 | - 18.9 | - 51.9 | n.a | n.a | n.a | + 41.0 | +103.8 | +25.5 |
| MOCAGE | - 46.6 | -22.8 | - 51.4 | - 7.0 | - 38.0 | - 1.0 | + 77.7 | +68.2 | +80.0 |
| UM-CAM | - 45.8 | - 9.2 | - 71.3 | - 59.5 | + 2.0 | - 69.0 | + 61.3 | +84.2 | +56.0 |
| Mean ± SD | - 61.1 ± 21.1 | - 35.5 ± 30.7 | - 70.2 ± 17.2 | - 47.1 ± 28.1 | - 37.6 ± 28.1 | - 47.9 ± 33.4 | + 70.5 ± 38.4 | + 92.5 ± 31.7 | + 65.6 ± 42.4 |

1073